

UNCLASSIFIED

AD 404 539

*Reproduced
by the*

DEFENSE DOCUMENTATION CENTER

FOR

SCIENTIFIC AND TECHNICAL INFORMATION

CAMERON STATION, ALEXANDRIA, VIRGINIA



UNCLASSIFIED

NOTICE: When government or other drawings, specifications or other data are used for any purpose other than in connection with a definitely related government procurement operation, the U. S. Government thereby incurs no responsibility, nor any obligation whatsoever; and the fact that the Government may have formulated, furnished, or in any way supplied the said drawings, specifications, or other data is not to be regarded by implication or otherwise as in any manner licensing the holder or any other person or corporation, or conveying any rights or permission to manufacture, use or sell any patented invention that may in any way be related thereto.

63-34

February, 1963

RADC-TDR-63-135

ASTIA DOCUMENT NO. AD-

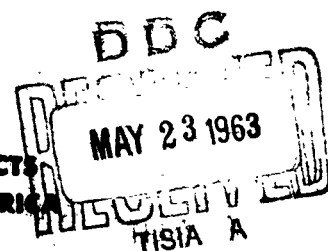
CATALOGED BY ACTIA
AS AD NO.
404533

404 539

FINAL REPORT
**STUDY OF THE GENERATION OF
COHERENT ELECTROMAGNETIC RADIATION
BY A
PULSATING PLASMA**

R. E. Skinner

APPLIED RESEARCH
DEFENSE ELECTRONIC PRODUCTS
RADIO CORPORATION OF AMERICA
CAMDEN, NEW JERSEY



ORIGINAL
REPRODUCED
COPY

Contract AF 30(602)2510

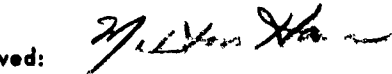
Prepared for
**ROME AIR DEVELOPMENT CENTER
RESEARCH AND TECHNOLOGY DIVISION
AIR FORCE SYSTEMS COMMAND
UNITED STATES AIR FORCE
GRIFFISS AIR FORCE BASE
ROME, NEW YORK**

Title of Report RADC-TDR-63-135

PUBLICATION REVIEW

This report has been reviewed and is approved.

Approved:



DAVID F. BARBER
Chief, Applied Research Laboratory
Directorate of Engineering

Approved:



WILLIAM P. BETHKE
Director of Engineering

FOR THE COMMANDER:



IRVING J. GABELMAN
Director of Advanced Studies

FINAL REPORT
STUDY OF THE GENERATION OF
COHERENT ELECTROMAGNETIC RADIATION
BY A
PULSATING PLASMA

R. E. Skinner

APPLIED RESEARCH
DEFENSE ELECTRONIC PRODUCTS
RADIO CORPORATION OF AMERICA
CAMDEN, NEW JERSEY

Contract AF 30(602)2510
Project Number 5561
Task Number 55183

Prepared for
ROME AIR DEVELOPMENT CENTER
RESEARCH AND TECHNOLOGY DIVISION
AIR FORCE SYSTEMS COMMAND
UNITED STATES AIR FORCE
GRIFFISS AIR FORCE BASE
ROME, NEW YORK

FOREWORD

This report concludes an unclassified research project by members of Applied Research, Defense Electronic Products, Radio Corporation of America. The project was supported by the Research and Technology Division of the United States Air Force Systems Command under Contract No. AF 30(602)2510. The Rome Air Development Center Project Engineer was J. Carroll.

The principal investigator was R. E. Skinner. The project leader was Dr. J. Vollmer.

PREFACE

In connection with a Rome Air Development Center program to investigate new techniques for generating large amounts of microwave power, this effort had the objective of investigating the microwave radiation produced from a plasma in a magnetic field. The experimental approach adopted was to utilize a modulated electron beam passing through the plasma as the excitation. A versatile, demountable, test setup for investigation of the radiation transverse to the modulated (five kmc/s) electron beam was designed and fabricated. The experimental setup was successfully operated, although the desired plasma frequency was not obtained due to excessive leakage of cesium gas from the interaction region.

The measurements taken during the test were statistically analyzed, and significant changes of about 20-db increase in the radiated-versus-transmitted signal were observed at several frequencies. This result was not expected since the operating frequency was above the plasma-cyclotron hybrid frequency.

ABSTRACT

Coherent radiation from a plasma stimulated by a modulated electron beam at frequencies above the hybrid frequency has been observed, with electronic gains of more than 20 db. The measurements were made in the 3.95-to 5.85-gc region. The cyclotron frequency was 2.90 gc and the hybrid frequency was less than 3.18 gc. The experiment was performed with a cesium plasma.

In this report the experiments, their results, and the experimental facilities are described. The facilities consist of an extremely versatile, demountable, bakeable vacuum system with a magnet which produces a highly uniform field over the region occupied by the plasma.

The results of this work are important and additional experimentation is recommended.

TABLE OF CONTENTS

	PAGE
ABSTRACT	i
NOMENCLATURE.....	viii
<u>SECTION</u>	
I Introduction	1/2
II Concept of the Experiment	3/4
III POD (Plasma Oscillation Diagnostic) Machine	5
A. General	5
B. Magnet	5
C. Vacuum System	12
D. Internal Support Structure	12
E. Bake-Out System	15
F. Refrigeration System	18
IV Experimental Arrangement	21
A. The Tube	21
1. Plasma Generation	21
a. Generator	21
b. Cesium Reservoir	23
2. Electron Gun, Couplers, etc.	26
B. Instrumentation	28
1. Microwave	28
2. Plasma Diagnostics	30

TABLE OF CONTENTS (Continued)

<u>SECTION</u>		PAGE
V	Experimental Results	33
	A. Microwave	33
	1. General Characteristics	33
	2. Cold and Semi-Cold Tube Data	35/36
	3. Hot Tube Data	47
	B. Plasma	56
VI	Conclusions and Recommendations	57/58
	A. Conclusions	57/58
	B. Recommendations for Future Work	57/58
	REFERENCES	59/60

LIST OF APPENDICES

APPENDIX		PAGE
I	Magnet Design	61
II	Magnet Supply Circuit	67
III	Cesium Filament Supply	69
IV	Cathode Activation Procedure	75/76
V	Statistical Analysis of Hot Tube Data	77

LIST OF ILLUSTRATIONS

<u>FIGURE</u>		PAGE
1	Basic Experiment	3/4
2	The POD Machine	6
3	Facility Block Diagram	7
4	Magnet Coil	9
5	Magnetic Field Plots	9
6	Schematic of Magnet Cooling System	10
7	Magnet Heat Exchanger System	10
8	Magnet Mounting	11
	A. Magnet Coil Clamp	
	B. Front View of Mounted Magnet	
	C. Right End View of Mounted Magnet	
9	Vacuum System Block Diagram	13
10	Vacuum Plumbing Line Sketch	14
11	Vacuum Vessel	14
•		
12	Vacuum Pumps	15
13	Basic Internal Support Structure	16
14	Bake-Out Temperature Vs. Time Plot for Right End Flange	16
15	Bake-Out Control Rack	17
16	Refrigeration Unit	19/20
17	Assembled Tube Structure	22
18	Cesium Filament and Heat Shield	23

LIST OF ILLUSTRATIONS (Continued)

<u>FIGURE</u>		PAGE
19	Temperature Distribution VS. Current for a Typical Tungsten Filament	24
20	Minimum Cesium Filament Life	25
21	Partially Assembled Cesium Reservoir	26
22	Electron Gun	28
23	Electron Gun Basic Circuit	27
24	Microwave Test Set-up	29
25	Disassembled Double Probe	31
26	Assembled Double Probe	31
27	Active Portion of Double Probe	32
28	Probe Circuitry	32
29	Cold Tube VSWR and Radiated Signal Relative to Input Signal	37/38
30	Semi-Cold Tube VSWR and Radiated Signal Relative to Input Signal	41/42
31	Semi-Cold Tube Transmitted Signal Relative to Input Signal	43/44
32	Semi-Cold Tube Transmitted Signal Relative to Radiated Signal	45/46
33	Hot Tube VSWR and Radiated Signal Relative to Input Signal	49/50
34	Hot Tube Transmitted Signal Relative to Radiated Signal	51/52
35	Hot Tube Transmitted Signal Relative to Input Signal	53/54
36	Geometry for Magnetic Field Calculations	62

LIST OF ILLUSTRATIONS (Continued)

FIGURE		PAGE
37	Calculated Normalized Magnetic Field Plot with α_1 as the Parameter	64
38	Magnet Supply	67
39	Magnet Supply Circuit	68
40	Cesium Filament Supply Circuit Diagram	70
41	Cesium Filament Supply Output Waveforms	71/72
42	Cesium Filament Supply	71/72

LIST OF TABLES

	PAGE
Table I Magnet Specifications	7
Table II Magnet Power Supply Specifications	8
Table III Refrigeration Unit Specifications	18
Table IV Some Typical Gun Operating Conditions with Magnetic Field (No Grid Modulation)	33
Table V Initial and Final Gun Operating Conditions for Data	34
Table VI Target and Actual Plasma Operation Conditions	47
Table VII Significant Points of Plasma Effect on Radiation	55
Table VIII Calculated Magnet Parameters	65
Table IX Cesium Filament Supply Specifications	73/74
Table X Gun Voltages and Currents - - No Magnetic Field	75/76

NOMENCLATURE

B = magnetic field

V_f = gun filament voltage

I_f = gun filament current

V_a = gun anode voltage

I_a = gun anode current

V_g = grid bias voltage

V_h = helix and drift tube voltages

I_d = drift tube current

I_{ms} = magnetic shield current

I_1 = input helix current

I_2 = output helix current

I_c = collector current

I_t = total current to drift tube, magnetic shield, helices,
collector and apertures.

f_c = cyclotron frequency

f_p = plasma frequency

$f_h = \sqrt{f_c^2 + f_p^2}$ = hybrid frequency

n_e = electron density

T_{res} = cesium reservoir temperature

T_i = ion temperature

T_e = electron temperature

SECTION I

INTRODUCTION

There is a steadily increasing demand for large amounts of microwave power. Sources presently available do not provide adequate power for many applications. Conventional techniques have apparently already reached, or are rapidly approaching, their basic limitations. One of these limitations is the output coupler problem; the high power densities involved often result in destruction of this device. It would thus be desirable to find a new method of coupling energy out of microwave generators. Another limitation is that the fine structures in conventional devices are damaged by high power densities. New structures are needed in which the mechanisms are microscopically large with fine structure effects being furnished microscopically.

Two mechanisms which offer properties capable of exceeding the above limitations are the interaction of an electron beam with a plasma, and the Cerenkov effect. The work reported here involves the study of the interaction of an electron beam with a plasma and the exploration of its use to obtain power higher than that available from conventional devices. To eliminate the output coupler problem, the concept is to use the generator as its own antenna (i.e., direct radiation).

It is well known that it is impossible to couple electromagnetic energy into or out of a homogeneous isotropic plasma. It is, therefore, imperative that the plasma be either inhomogeneous or modified in some such manner as to produce an anisotropy. An anisotropy can be produced by the application of a magnetic field.

It is also known that an electron beam passing through a plasma can lead to rapidly growing waves in a manner somewhat analogous to a traveling wave tube. The growth constant, though, is much larger than in any traveling wave tube.¹⁻⁶ Kino⁶⁻⁷ and Skinner⁸ have independently suggested that this growing wave can be made to radiate directly from the plasma. The prime purpose of the present investigation was to experimentally ascertain whether or not this is indeed the case. The experimental approach was thought to be better than a theoretical approach at this time because the latter involves extremely complex mathematics and a variety of arbitrary assumptions.

SECTION II

CONCEPT OF THE EXPERIMENT

The basic concept of the experiment, although quite simple, was found to be difficult to execute. The experimental arrangement is illustrated in Figure 1. It is seen to consist of the passage of a modulated electron beam through a plasma located in an axially magnetic field, with a detector for radiation. The parameters of the experiment are the type of plasma, plasma density (n) — or plasma frequency (ν_p) — magnetic field (B), beam voltage (V), beam current (I), and modulation frequency (ν). Also involved is the shape and uniformity of the magnetic field. To eliminate one parameter, one might make the applied magnetic field uniform over the plasma.

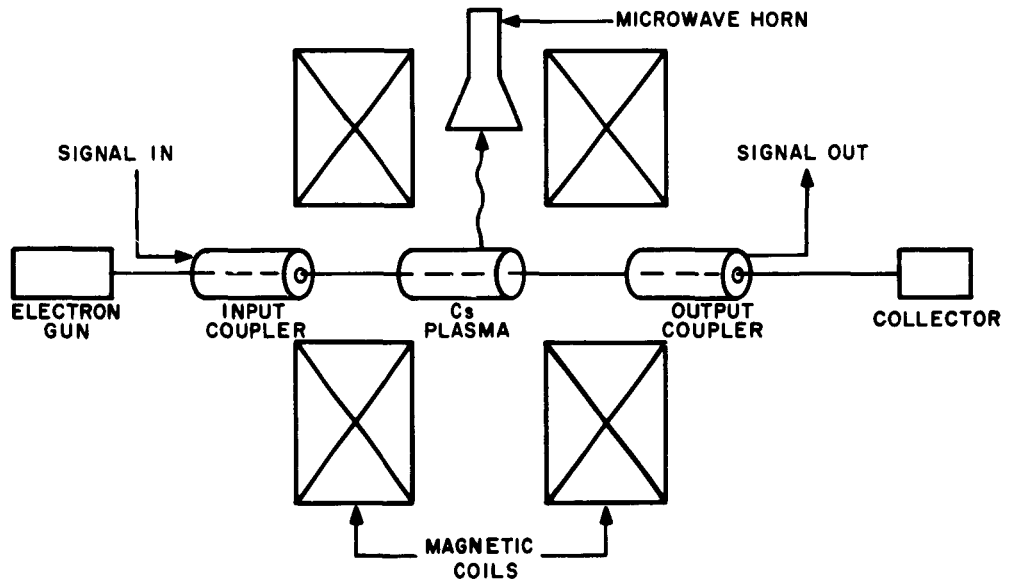


Figure 1. Basic Experiment

SECTION III

THE POD (Plasma Oscillation Diagnostic) MACHINE

A. GENERAL

The original plan was to build a sealed-off tube incorporating the electron gun, input coupler, plasma, output coupler, and the collector. However, a closer examination of the experiments involved convinced us that a demountable tube would be preferable in the long run. This is so for the following reasons:

1. Greater versatility and lower initial cost.
2. Ease of changing the parts configuration.
3. Lower cost for changing the parts configuration.
4. Quick replacement of cathodes.
5. Less techniques development.

As an example of the increased versatility at lower cost, one can easily visualize the ability to completely change the internal works in a week or two, with the help of modelmakers, at a fraction of what it would cost to build one sealed-off tube. The basic facility that evolved has been nicknamed the "POD Machine". A picture of the assembled machine is shown in Figure 2.

In Figure 3 a block diagram of the POD Machine is shown. It is seen to consist of a bakeable vacuum system, the magnet and associated equipment, equipment for bake-out, the refrigeration system to cool the walls (to ensure that the cesium plasma which escapes is condensed out in the desired spot), the plasma device itself, and associated equipment. The associated equipment includes the device power supply, plasma generation equipment, microwave test equipment, and plasma diagnostic equipment. The general design calls for a uniform magnetic field of up to 3.5 kilogauss (cyclotron frequency of 10 Gc), an ultimate vacuum of 10^{-8} torr, and as many experimental ports as feasible. One of these ports is for a microwave horn for frequencies as low as H-band (3.95 to 5.85 Gc). A major advantage of this system is a wide range of experimental configurations for the plasma device. In the following sections, each of the items making up the POD Machine is described in more detail.

B. MAGNET

The details of the magnet design are covered in Appendix A. The requirement that the vacuum vessel have a port capable of handling an H-band horn located at the

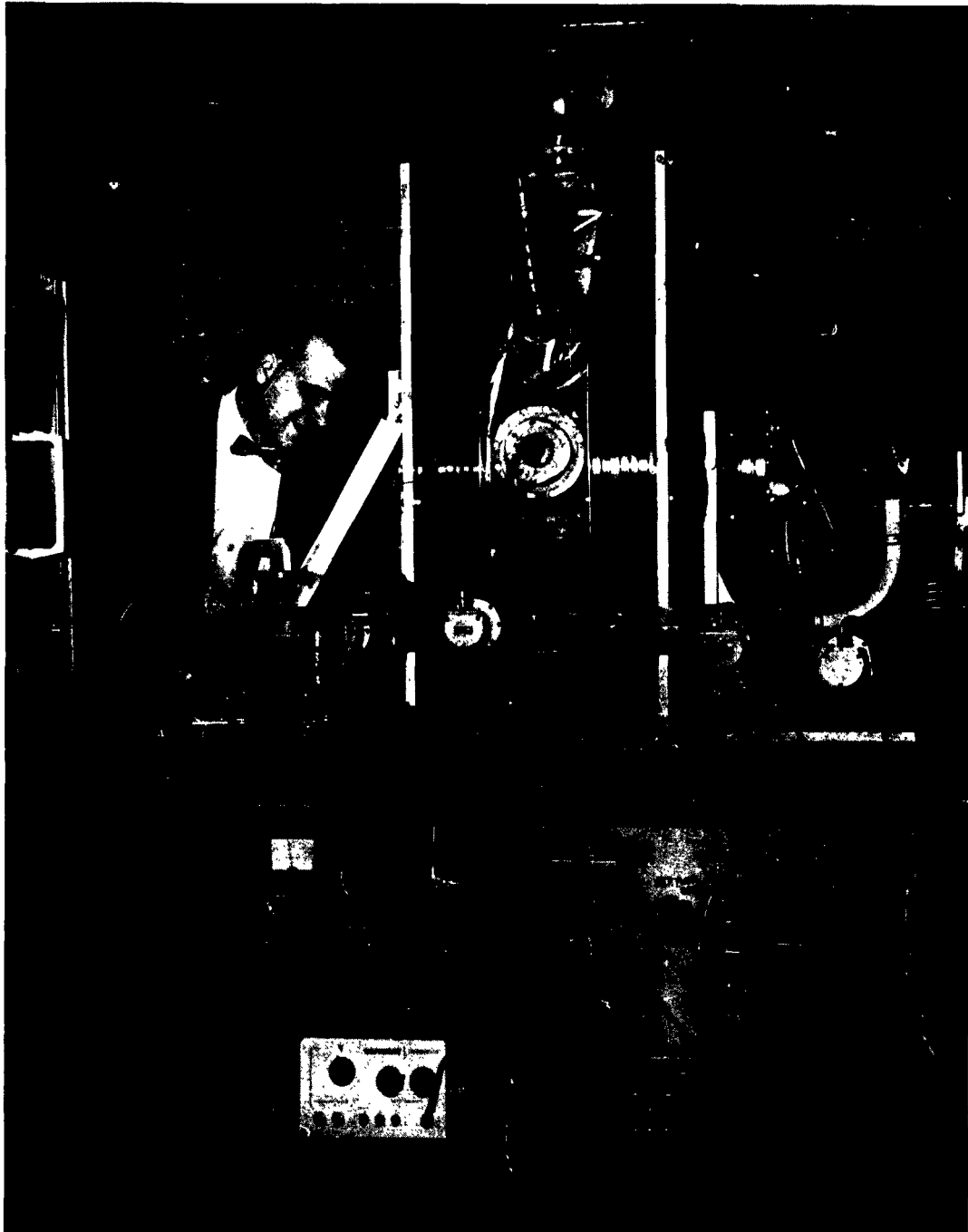


Figure 2. The POD Machine

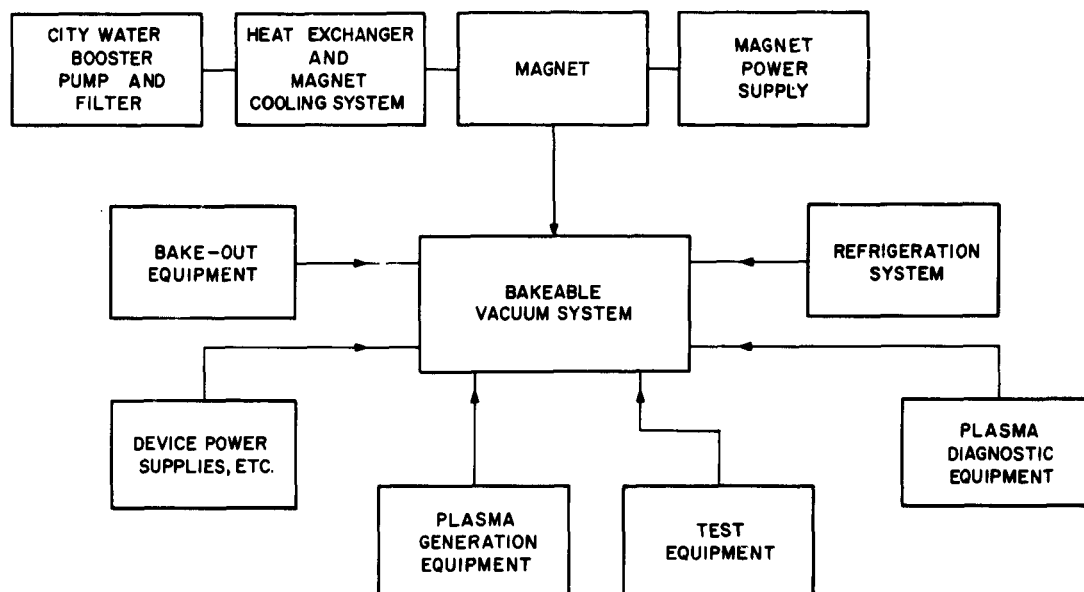


Figure 3. Facility Block Diagram

center of the magnetic field led to a gap of 7.375 inches at its center. It was further required that the magnetic field be uniform to better than 1% along the axis in the gap between the coils. The specifications on the resultant magnet are given in Table I.

TABLE I

MAGNET SPECIFICATIONS

Inside Diameter	14.0 in.
Outside Diameter	36.4 in.
Pancake Coil Thickness650 in.
Section Thickness	4.550 in.
Gap Size	7.375 in.
Over-all Length	18.47 in.
Field	0-3.57 kg
Voltage	0-310 volts
Current	0-250 amps
Power	0-80 KW
Temperature Rise	50° C
Inlet Temperature	30° C
Pressure Head	90 psi

TABLE I (Continued)

MAGNET SPECIFICATIONS

Coolant Flow Rate	Calculated requirement = 5.7 gpm — actual = 4 gpm
Single Coil Resistance090 ohm
Insulation Test	5 volts/turn, 1500 volts highpot
Pressure Test	1000 psi hydrostatic

The magnet consists of 14 pancake coils -- Figure 4 -- seven on each side of the gap. The pancake coil is wound with 73 turns of 0.270-inch-square bare copper wire with a 0.183-inch-diameter hole for passage of the coolant. Each coil contains about 500 feet of wire. Insulation is provided by 0.015-inch fiberglass tubing pulled over the wire, and a 0.010-inch-thick epoxy fiber-glass-impregnated disc between the two windings. The whole coil is vacuum-impregnated with Shell No. 828 epoxy compound. The 14 pancakes are connected electrically in series with the coolant passing through the coils in parallel.

Plots of the magnetic field on the Z axis, along the radial midplane, and along an axis parallel to the radial midplane at the edge of the gap have been made. These are shown in Figure 5. It is seen that the field along the axis over the gap is flat to better than three-quarters of 1%, and that the field over the region occupied by the plasma (three inches long and one inch in radius) is constant to within half of one percent.

The cooling system is illustrated schematically in Figure 6. A picture of the heat exchanger system is shown in Figure 7.

Each half of the coil is mechanically clamped between an aluminum plate one inch thick and a stainless steel "hat-like" assembly — Figures 8a, b and c. The specifications on the magnet power supply are given in Table II and the design of the power supply is discussed in Appendix B.

TABLE II

MAGNET POWER SUPPLY SPECIFICATIONS

Line Voltage	220V, 3 ϕ
Output Voltage	0-312 VDC
Output Current	0-203 Amps DC
Ripple	4%, 360 cycle
Output Power	63 Kw



Figure 4. Magnet Coil

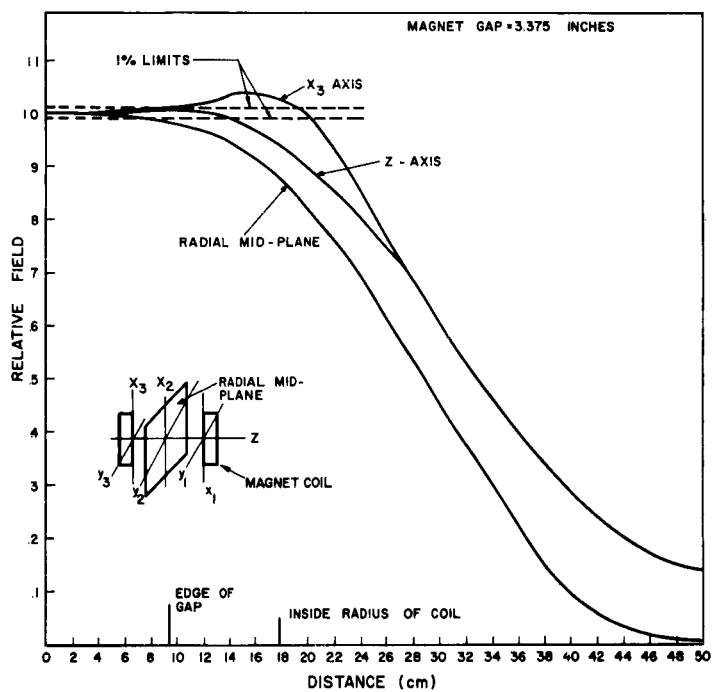


Figure 5. Magnetic Field Plots

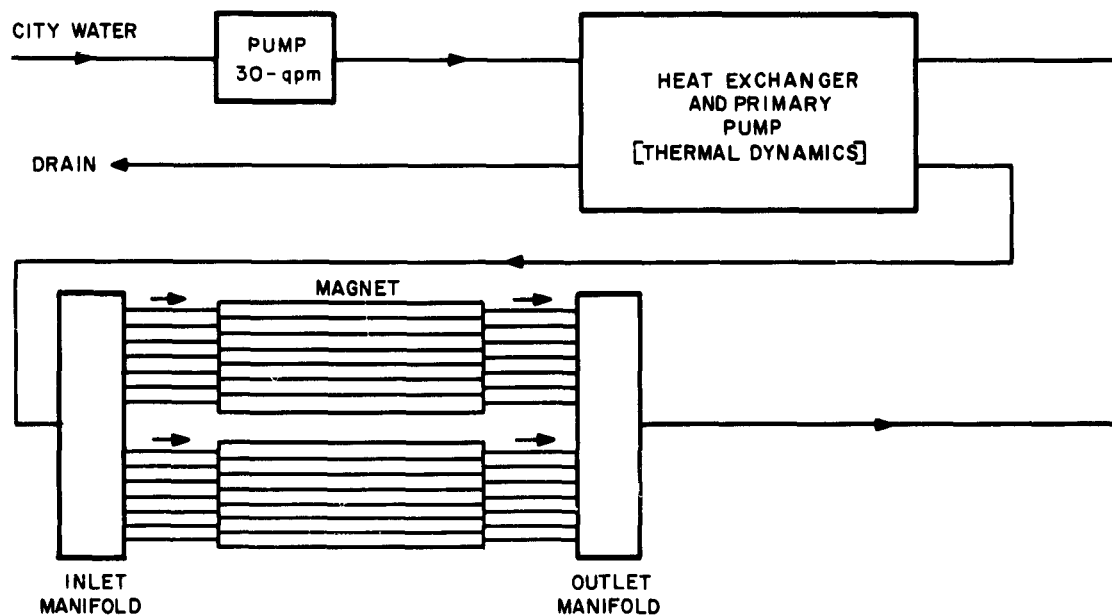


Figure 6. Schematic of Magnet Cooling System

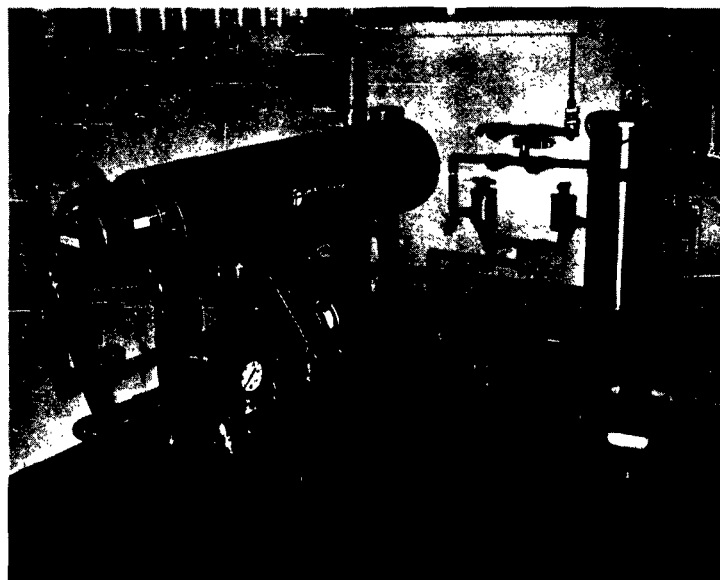
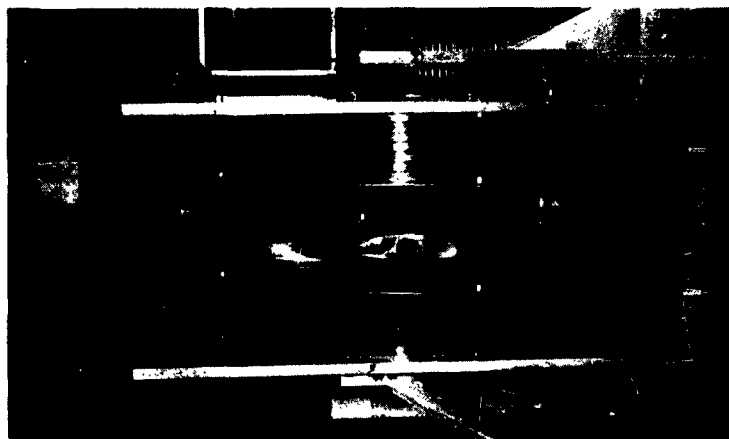


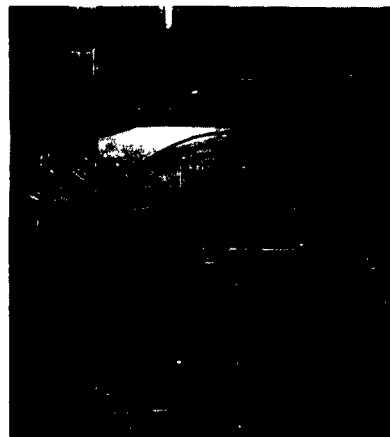
Figure 7. Magnet Heat Exchanger System



A. Magnet Coil Clamp



B. Front View of
Mounted Magnet



C. Right End View of
Mounted Magnet

Figure 8. Magnet Mounting

C. VACUUM SYSTEM

The requirements imposed on the vacuum system are that it be capable of producing a vacuum up to 10^{-8} torr, have experimental ports capable of housing a microwave horn at H, C or X band, have cross ports for millimeter wave plasma diagnostic equipment, a port capable of use with a double probe and/or a window and a port for entry of plasma generation equipment. Also, it must provide high voltage feedthroughs for supplying voltages to the electron gun, high current feedthroughs for feeding power to heaters for generation of plasmas by contact ionization, feedthroughs for feeding microwave energy to the input coupler and from the output coupler, and means whereby the electron gun portion is pumped as independently from the rest of the vessel as feasible. The block diagram of the resultant vacuum system is shown in Figure 9. A line drawing (not to scale) of the vacuum plumbing is shown in Figure 10. The vessel is pumped at both ends, which are connected to a common pump under the table where the vessel is mounted. A baffle plate between the electron gun and the rest of the device ensures that any cesium released will have as long a path as possible to get to the gun portion of the device.

A picture of the vacuum vessel is shown in Figure 11. The two horizontal tubes furnish the ports for millimeter wave diagnostics. The square vertical port is for handling the microwave horn, the oblique port is capable of handling the window shown, or a double probe. The small port underneath the vessel is for the cesium reservoir. All of the power lead feedthroughs are located on the right end flange, along with the coax feedthroughs for feeding microwave energy to and from the couplers. Also visible are the cooling coils used to cool the wall of the vessel. This ensures that cesium will condense on the wall and not elsewhere. To date the best vacuum attained has been 10^{-6} torr. This is a result of a damaged shear surface on the left end flange which has not been feasible to correct at this time. All of the seals above the cold trap (that is, on the baked portion of the vessel) are of the copper shear type. The vessel and piping are made of 304 Stainless Steel. A picture of the pump portion of the vacuum system is shown in Figure 12.

D. INTERNAL SUPPORT STRUCTURE

The internal support structure is mounted on the right end flange and supports the various parts of the tube structure at the appropriate positions. The basic internal support structure is shown in Figure 13. It is designed so that various size plasma regions, various length helices, and various types of couplers can be accommodated. A change in any one of these requires a modification of a minimal number of parts with a minimum amount of machining. The internal support structure is fabricated from 303 and 304 Stainless Steel and aluminum.

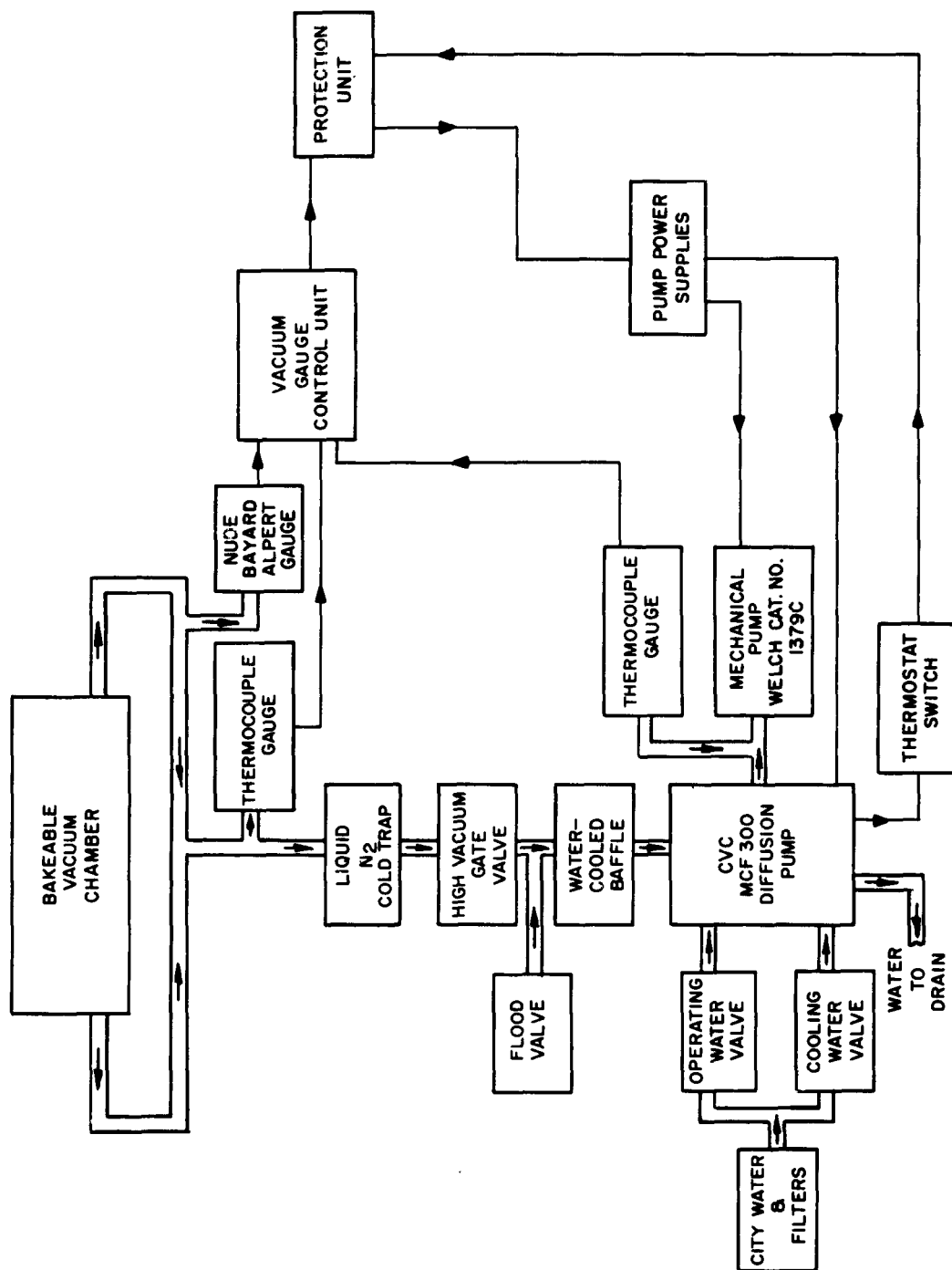


Figure 9. Vacuum System Block Diagram

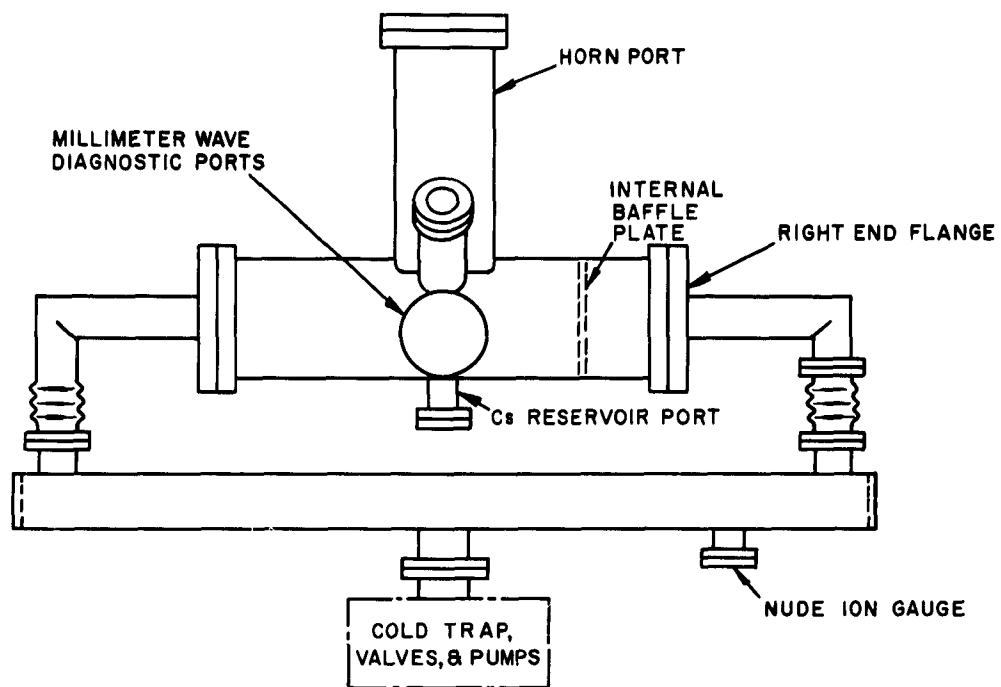


Figure 10. Vacuum Plumbing Line Sketch



Figure 11. Vacuum Vessel



Figure 12. Vacuum Pumps

E. BAKE-OUT SYSTEM

Bake-out is accomplished by 19 separately controlled heaters. The heaters for the cylindrical portions of the vessel are made out of Brisquet-type heater tape of varying lengths connected in parallel and in series. The heaters for the flat flanges are specially made. Insulation is provided by one to three inches of house-type fiberglass insulation. The average power density is about 100 watts per square foot. The one exception from using fiberglass for insulation is the use of quarter-inch-thick asbestos insulation on the sides of the horn port tube. Here the power density runs to 1,400 watts per square foot. Temperatures are monitored by 72 thermocouples located at strategic points over the vessel. In particular, each of the small flange joints is provided with four thermocouples, two on each side of the joint; the big flanges have three thermocouples on each side of the joint with one thermocouple in the center of the flat surface. The bake-out system is designed to take the vessel to a maximum temperature of 400° C. The main design consideration was to provide the means of ensuring that the temperature gradient across the flanges be kept as small as possible, preferably to less than 10° C. For the experiment reported here, the vessel was baked out at a temperature of 200° C. A typical time-temperature plot for a thermocouple located on the right end flange is shown in Figure 14. The bake-out control rack is shown in Figure 15.

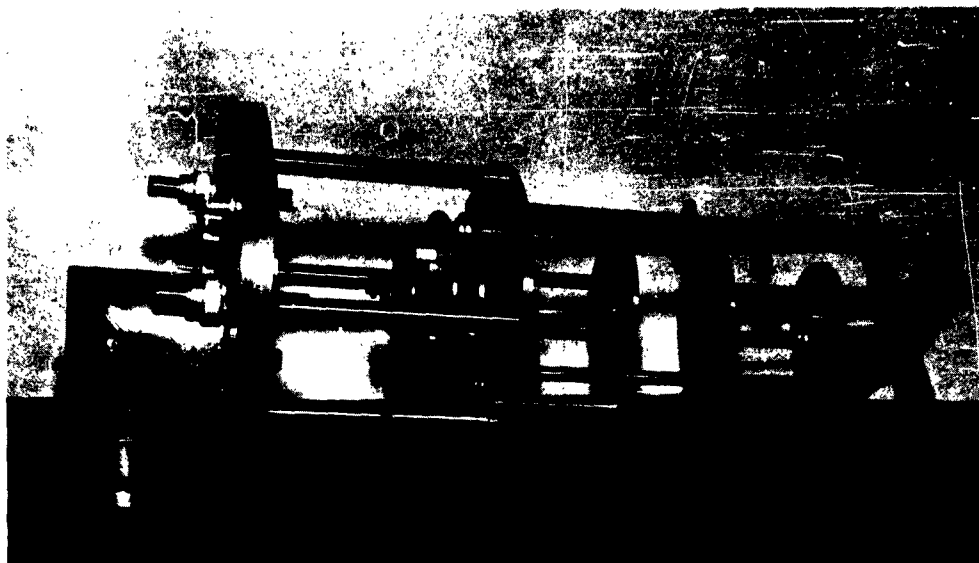


Figure 13. Basic Internal Support Structure

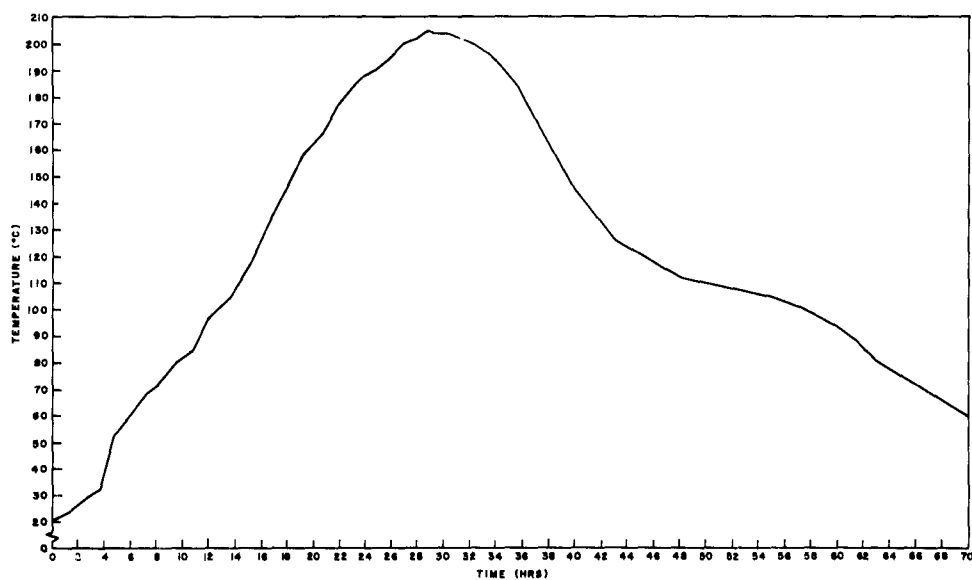


Figure 14. Bake-out Temperature vs Time Plot for Right End Flange

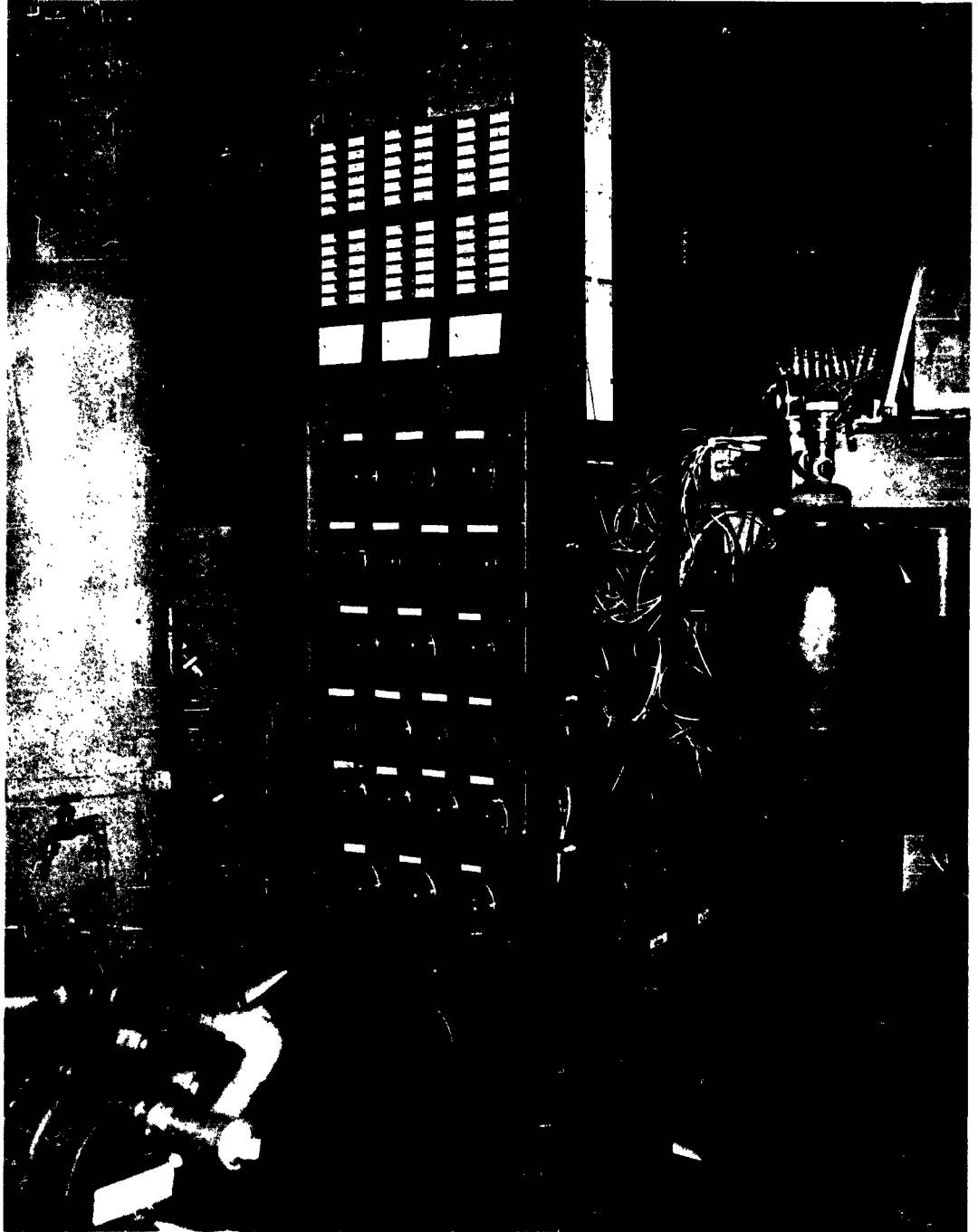


Figure 15. Bake-Out Control Rack

F. REFRIGERATION SYSTEM

The basic requirements for the refrigeration system were to cool the vessel walls to a temperature of -20°C , with up to a 3.5 kw heat load. This high heat load was imposed in anticipation of the possibility of going to plate-type contact ionization surfaces similar to those in the Q Machine at the Princeton Plasma Physics Laboratory. The detailed specifications of the refrigeration system are given in Table III.

A picture of the refrigeration unit is shown in Figure 16. The system uses a 50% ethylene glycol water mixture for circulation through the cooling coils on the vacuum vessel walls. A bonus derived from this refrigeration unit is cryogenic vacuum pumping by the cold walls of the vessel.

TABLE III

REFRIGERATION UNIT SPECIFICATIONS

Primary Coolant	50% Ethylene Glycol Water Solution
Temperature	-25°C
Heat Load	0-3.5 kw
Coolant Flow Rate	4 gpm
Coolant Pressure	20 psi
Cool Down Time	4 hrs
Primary Power	220 V, 3 ϕ , 60 cycle
Secondary Coolant	City Water at 4 gpm

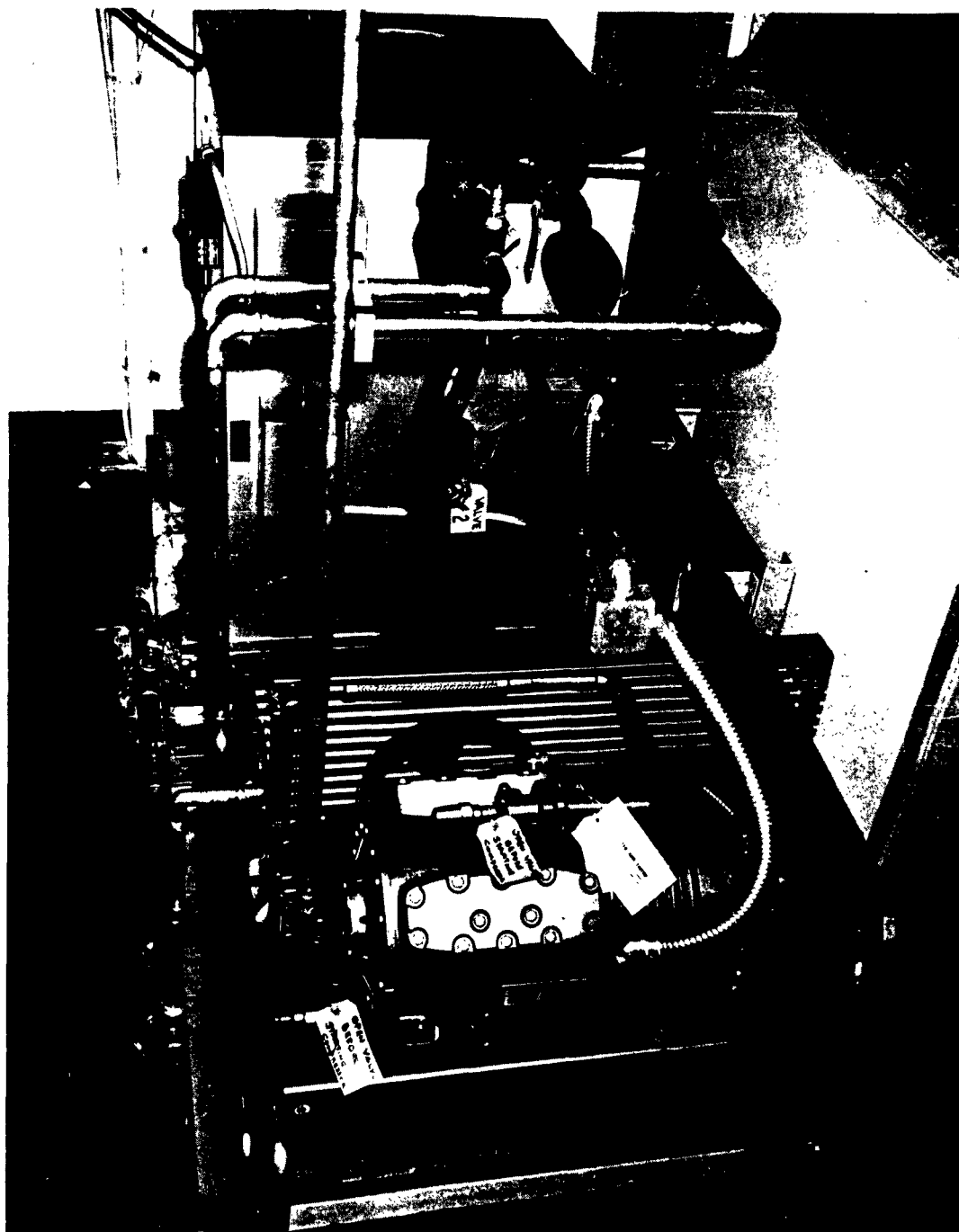


Figure 16. Refrigeration Unit

SECTION IV

EXPERIMENTAL ARRANGEMENT

A. THE TUBE

The completely assembled tube and internal support structure is shown in Figure 17. Just below the big baffle plate at the middle of the photograph is the electron gun mounted on its platform. The input coupler and helix are located on the opposite side of this plate. Above this plate and between the two stainless steel discs is located the plasma generation region. Next come the output helix and coupler and, finally, the collector.

1. Plasma Generation

A cesium plasma generated by contact ionization was chosen for two reasons: 1) lack of noise and 2) high ionization percentage.^{6,9} In general, if nonlinear effects are to be avoided, the ionization percentage should be as high as possible, preferably 100%. In as much as it is also desirable for the plasma to be as free of noise as possible, a quiescent plasma should be used.

a. Generator

The plasma generator consists of two tungsten filaments and their heat shields located at opposite ends of a cylindrical region surrounded by a quartz tube two inches in diameter. The tungsten filaments (spiral wound pancakes) are made from 0.062-inch-diameter tungsten wire. One of the filaments with its heat shield is shown in Figure 18. The filament is supported by and current-fed through two molybdenum support rods. These support rods have a necked-down region of appropriate length and diameter to prevent heat sinking of the filament. The temperature-vs-current characteristics for a typical filament are shown in Figure 19. The running parameter is the position on the spiral. It is important that the temperature of the molybdenum support rods be kept as low as possible. If they are allowed to become too hot, the molybdenum evaporates from the support and deposits itself on the walls of the quartz tube, decreasing the heat loss and resulting in the eventual melting of the support. This happened with the first set of support rods used. A lower limit on the life time of the filament can be calculated by assuming: 1) that the useful life of the filament is the time required to deposit a monomolecular layer of molybdenum on the quartz tube; 2) that a molecule of molybdenum contains 8 atoms; and 3) such a molecule is about 5 Å square. The resulting lifetime as a function of temperature is shown in Figure 20. At 1850° K the lifetime is seen to be about 14 hours. Further, the plot shows that the lifetime on this basis decreases almost exponentially with increasing temperature. Experimentally, the filaments have been run for over 12 hours at 2000° K center temperature with no measurable plating.

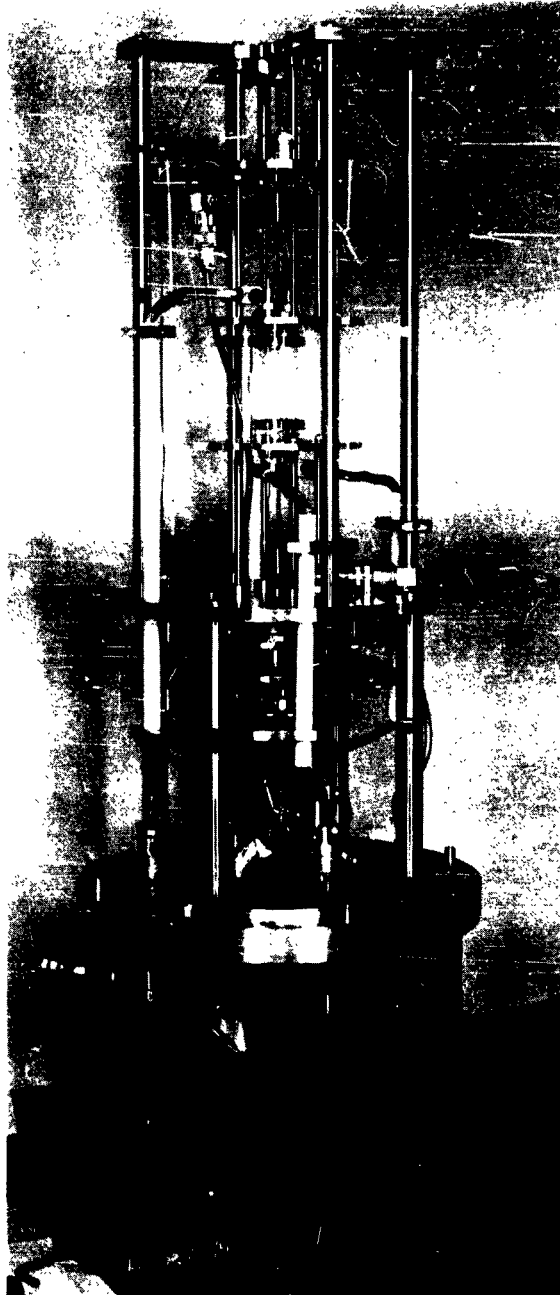


Figure 17. Assembled Tube Structure

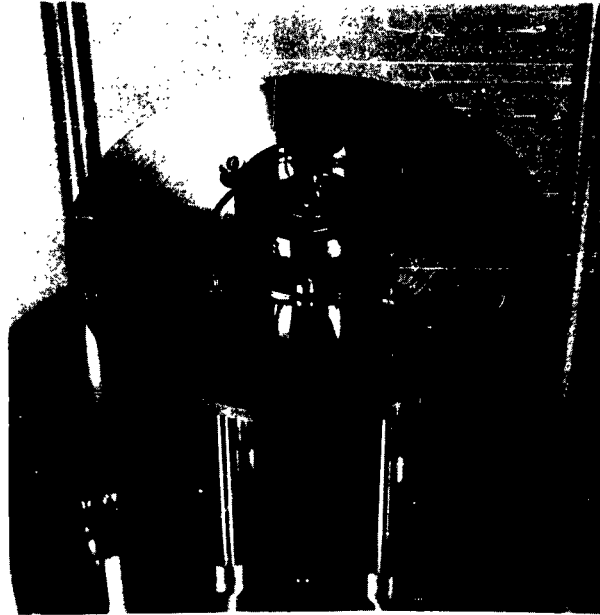


Figure 18. Cesium Filament and Heat Shield

For this experiment the filaments are operated at approximately $2,000^{\circ}\text{K}$ with the supports at 1850°K . The voltage drop across the filament is less than 3.2 volts rms, or 6.4 volts peak. With the filament transformer center-tap grounded, the peak voltage to ground is less than 3.2 volts. This in turn minimizes the possibility of voltage break-down between portions of the filament or from the filament to ground in the cesium atmosphere.

The plasma generation system is operated in the vapor pressure mode, with cesium vapor being supplied from a reservoir maintained at constant temperature through a feed tube. The cesium filaments are powered by a half-wave-rectified nonfiltered 400-cycle power supply (see Appendix C). This heating current flows for 2.5 ms and then is off for 2.5 ms.

b. Cesium Reservoir

A view of the cesium reservoir before it was completely assembled is shown in Figure 21. The reservoir consists of a water-jacketed chamber mounted on a 2-inch flange by means of thin wall (.010 inch) stainless steel tubes. The mounting is designed in such a manner as to minimize heat transfer between the water jacket and the flange, thereby ensuring constant temperature operation. Inside the chamber is located a cup/knife arrangement. The cup is driven by a drive rod through a bellows.

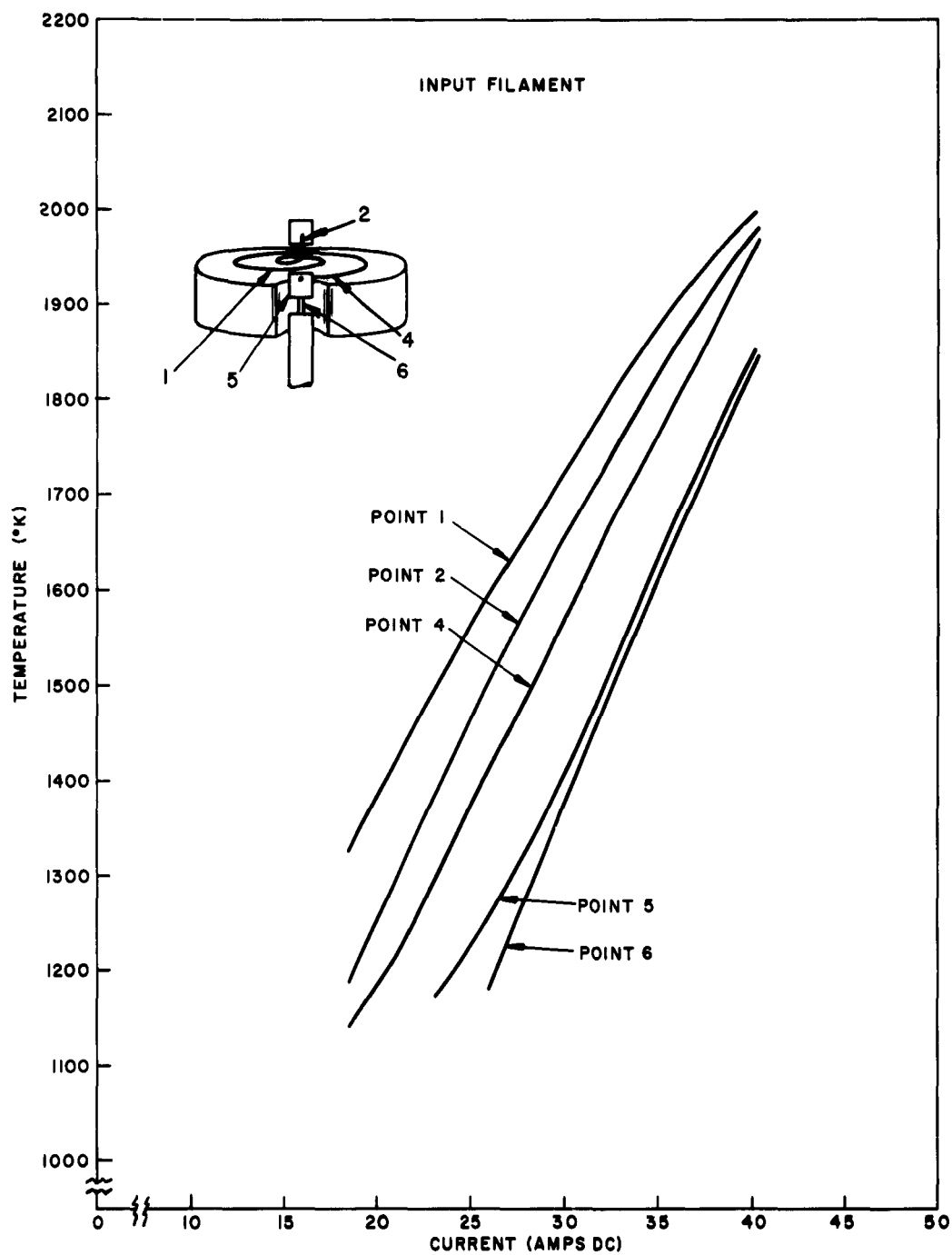


Figure 19. Temperature Distribution vs Current for a Typical Tungsten Filament

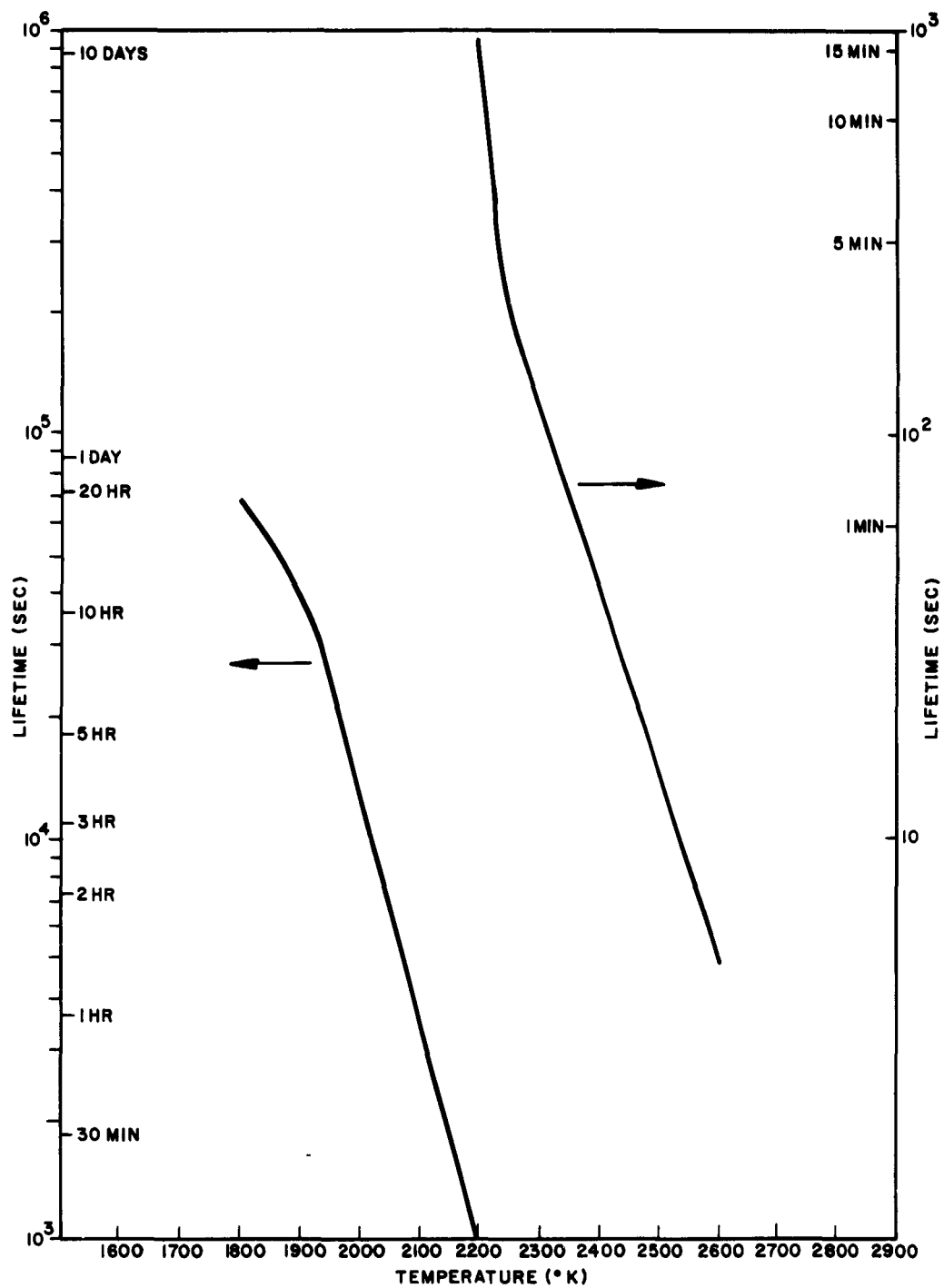


Figure 20. Minimum Cesium Filament Life

This mechanism provides a means of breaking the vial containing the cesium at the desired point in the experiment. The cesium vapor is fed to the plasma chamber through a hole in the quartz tube by means of a Pyrex chimney. The water jacket is fed from an E. H. Sargent Cat. No. S-82055 constant temperature bath capable of maintaining the temperature constant to $\pm 0.01^\circ\text{C}$.

2. Electron Gun, Couplers, etc.

The electron gun is a convergent type, and is the one used in the RCA Type 1137 traveling wave tube. It is shown mounted on part of its platform in Figure 22. The complete platform assembly for the gun provides two independent motions at right angles to each other and to the tube axis. It further allows independent motion along the axis and tilting of the gun axis with respect to the tube axis. This movement permits the gun's axis to be carefully aligned with the axis of the rest of the tube. When the gun is in position it is located inside a magnetic shield mounted on the baffle plate of the tube structure on stand-off insulators. The basic electrical circuit for the operation of the electron gun beam system is shown in Figure 23.

The cathode is oxide-coated with a mixture of BaO, SrO, and CaO. No apparent problems of cathode contamination have been encountered. The system was operated for 2-1/2 months before cathode activation and for 2-1/2 weeks after activation.



Figure 21. Partially Assembled Cesium Reservoir

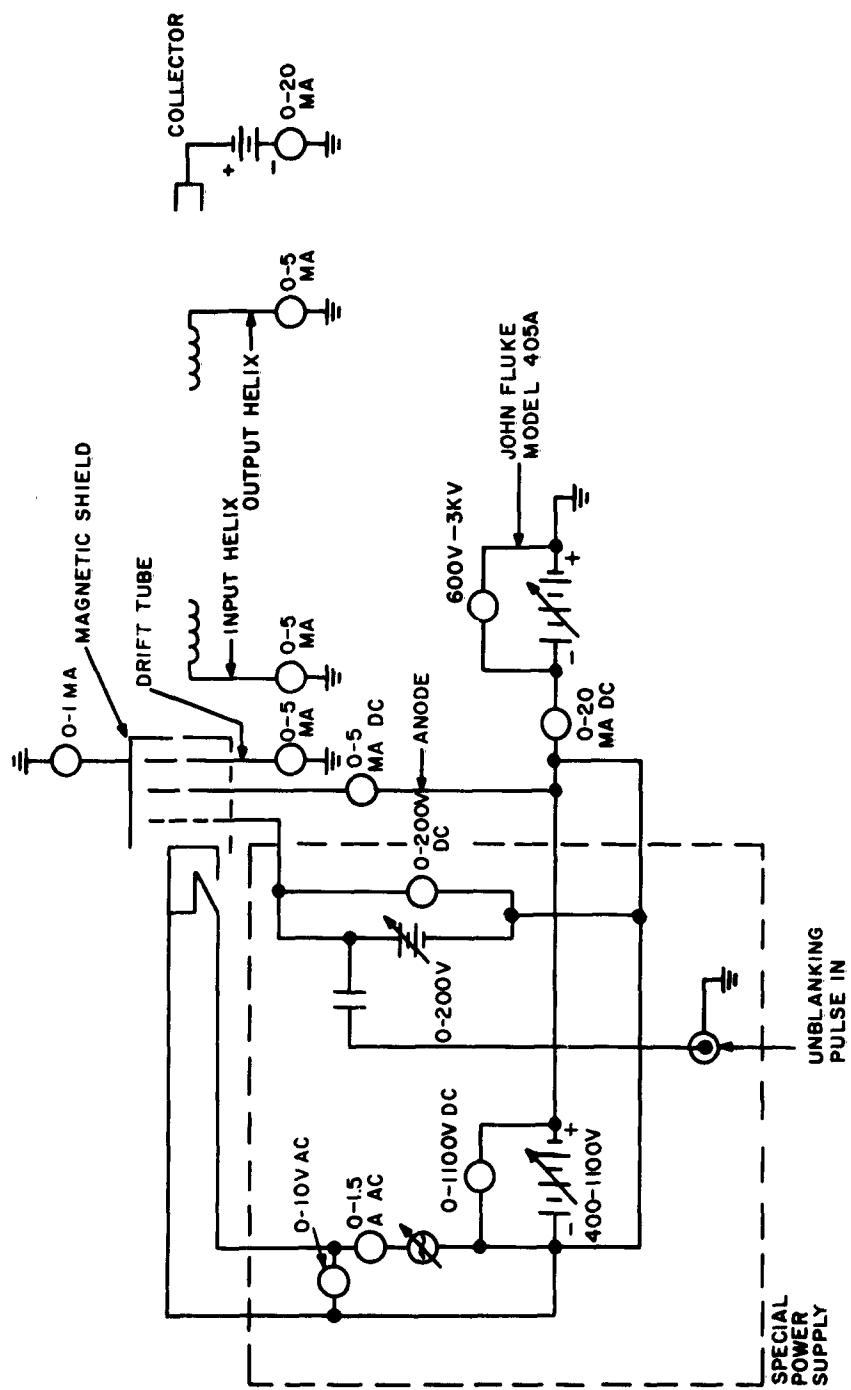


Figure 23. Electron Gun Basic Circuit



Figure 22. Electron Gun

The couplers and helices are taken from an RCA Developmental Traveling Wave Tube Type A1189. The helices are .110 inch in diameter, and have 41.2 TPI; they are made of silver-plated 0.010-inch-diameter tungsten and are imbedded in the glass helix tube. Each of the helices has an active length of 3.4 inches and is coated with 1.5 inches of Aquadag at the end opposite the coupler. This amount of Aquadag gives about 4.5 db of attenuation on each helix. Special couplers capable of taking bake-out at 400° C were ordered but have not been delivered yet. The temperature limit of the present couplers is between 200° C and 250° C.

The radiation detector system consists of a Narda Cat. No. 643 H-band horn. In order to get the horn inside the port tube, it was necessary to cut off the large end so that the opening is now 6.00 inches by 4.46 inches. The horn is aligned with the electric field parallel to the applied magnetic field. It is located with its flange 15.1 inches from the axis of the plasma.

B. INSTRUMENTATION

1. Microwave

A block diagram of the test set-up used to make the microwave measurements is shown in Figure 24. All measurements are normalized for an input power of two milliwatts. The radiation detection crystal and its associated SWR amplifier were calibrated

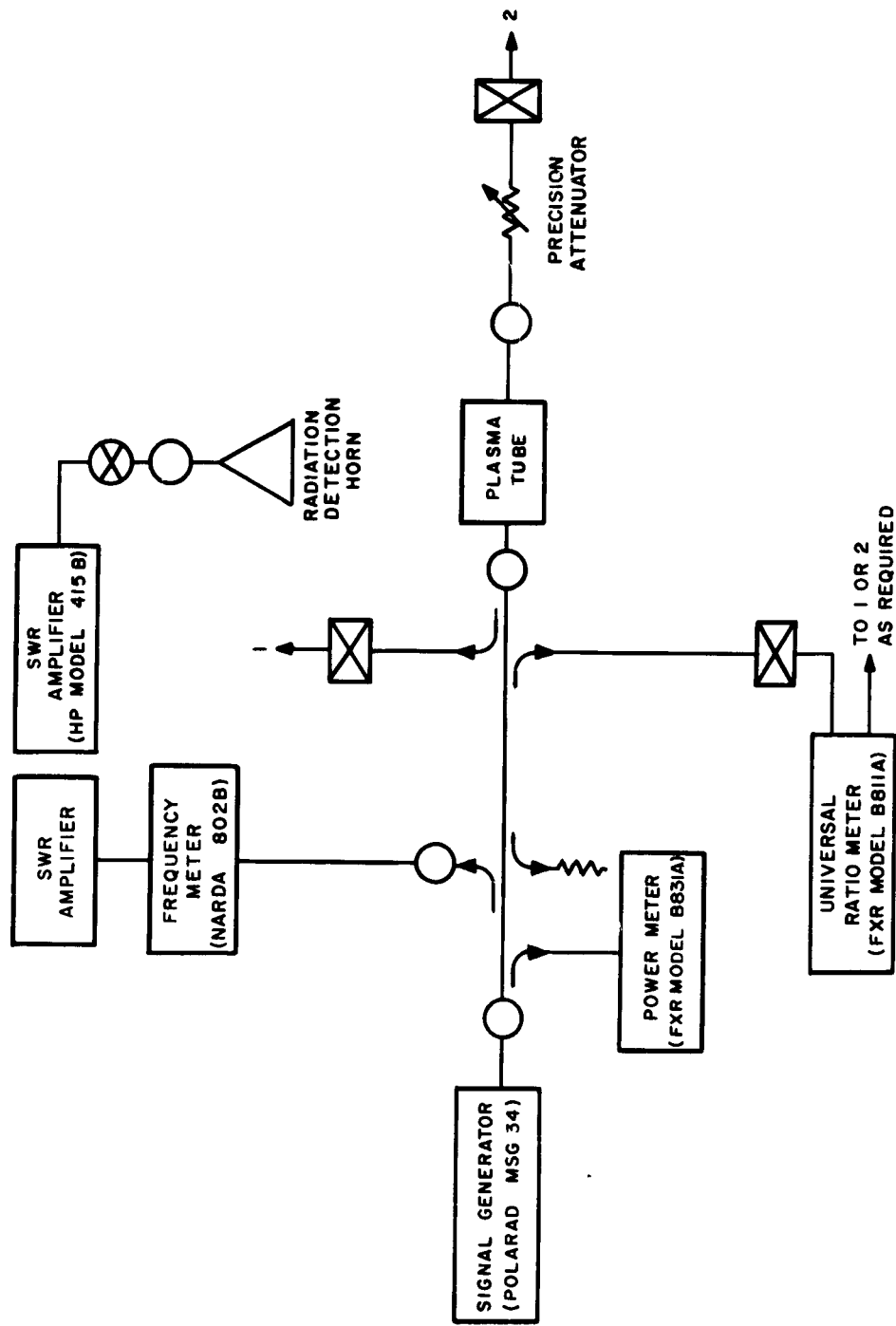


Figure 24. Microwave Test Set-up

as a function of input power and frequency. The radiation measurements were then made in terms of the threshold sensitivity of the detection set-up, i.e., crystal plus SWR amplifier. This in turn was translated to db down with respect to a normalized power input of two milliwatts. All measurements were made on a point-to-point basis.

2. Plasma Diagnostics

Original plans called for plasma diagnostic measurements using both millimeter wave diagnostic techniques and a double probe. In the interest of scheduling, the millimeter wave diagnostics were eliminated from this phase of the program. The double probe is a modification of that used by N. Rynn on the Q machine at the Princeton Plasma Physics Laboratory. A picture of the probe disassembled is shown in Figure 25, and the assembled probe is shown in Figure 26. The active portion of the probe is illustrated in Figure 27. It is seen to consist of a molybdenum cylindrical electrode 1.57 millimeters long and 1.22 millimeters in diameter, with a second 0.762-millimeter-diameter tungsten electrode protruding from its end by 1.35 millimeters. Thus, the area of the cylindrical electrode is .0602 square centimeters and the area of the tungsten electrode is .0323 square centimeters. The circuitry for the double probe is shown in Figure 28. The P6000 probes have an input impedance of 10 Megohms to ground. This leaves a net impedance to ground of 2.5 Megohms, which is less than optimum but still useable. A Mosely 2D X-Y recorder was also used. The frequency response of the system is limited by the capacity of the coaxial cables shunting the equivalent resistance of the double probe. It was necessary to position the scope as far from the magnet as possible, thus, giving a shunt capacity between the cables of about 250 micromicrofarads. The shunt capacity of the probe itself is 45.8 micromicrofarads. This capacity can present problems in the form of phase shift and extraneous currents if the plasma density is too low and the plasma equivalent resistance is hence too high. Problems with the 400-cycle pickup on the probe were also encountered with the plasma present.



Figure 25. Disassembled Double Probe

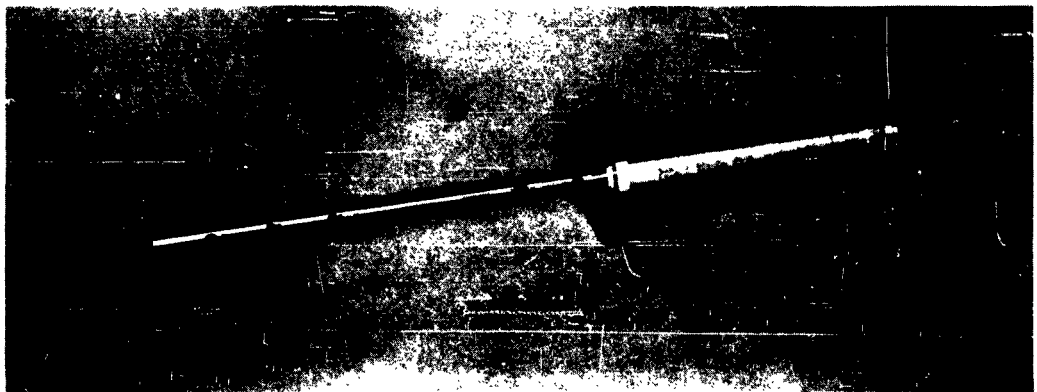


Figure 26. Assembled Double Probe

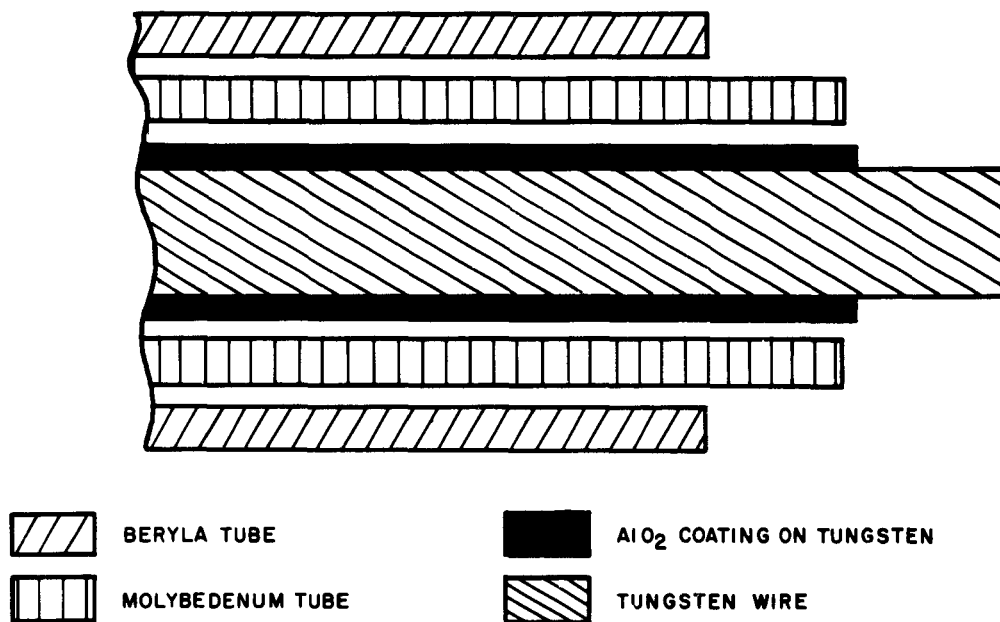


Figure 27. Active Portion of Double Probe

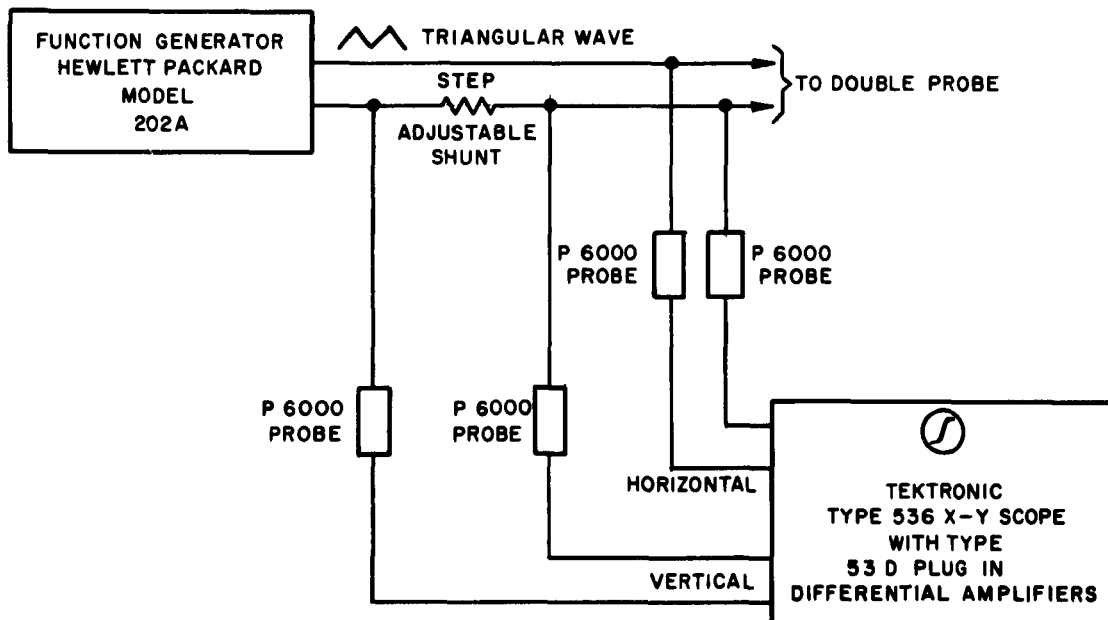


Figure 28. Probe Circuitry

SECTION V

EXPERIMENTAL RESULTS

A. MICROWAVE

1. General Characteristics

Emission from the cathode was low, but adequate. There is a definite indication that the emission constant never reached the value specified for the cathode used. This was apparently due to the low activation temperatures produced by the activation procedure. Since the cathode was not visible in the assembled POD machine, an empirical activation procedure of conservative nature was developed. This procedure is described in Appendix IV.

Initial gun-electrode voltages and currents for two different fields are given in Table IV. No problem was encountered in aligning the tube axis with the magnetic field axis. Some problem with arc-over in the gun was encountered with a magnetic field of 600 gauss at a helix potential of 1.2 kv. An upper operating limit was fixed at 1.1 kv.

TABLE IV

SOME TYPICAL GUN OPERATING CONDITIONS WITH MAGNETIC
FIELD (NO GRID MODULATION)

B	$=$	1456 gauss	V_h	$=$	1253.2 volts
V_f	$=$	8.8 vac	I_d	$=$	1.8 ma
I_f	$=$	1.42 amps ac	I_{ms}	$=$	0 ma
V_a	$=$	607 volts	I_1	$=$	0 ma
I_a	$=$	5 ma	I_2	$=$.4 ma
V_g	$=$	-14 volts	I_c	$=$	2.8 ma
			I_t	$=$	4.7 ma

TABLE IV (Continued)

SOME TYPICAL GUN OPERATING CONDITIONS WITH MAGNETIC
FIELD (NO GRID MODULATION)

B = 1032 gauss	V _h = 1010 volts
V _f = 8.8 vac	I _d = 2 ma
I _f = 1.42 Amps ac	I _{ms} = 0 ma
V _a = 607 volts	I ₁ = 0 ma
I _a = 4.6 ma	I ₂ = .45 ma
V _g = -15 volts	I _c = 2.8 ma
	I _t = 4.6 ma

Experimentation showed that for a given magnetic field there exists an optimum helix voltage for best collector current and an optimum helix voltage for best microwave transmission. These voltages are not necessarily the same. The helix voltage used in obtaining the reported results was the one which gave maximum transmission at a frequency of 4.96 Kmc.

The initial and final gun operating conditions used in obtaining the reported microwave data are given in Table V. Note that the anode current and drift tube current decreased slowly during most of the experiment (over a period of about three weeks) while the collector current remained constant.

TABLE V

INITIAL GUN OPERATING CONDITIONS FOR DATA

B = 1032 gauss	I _d = 1.6 ma
V _f = 8.8 vac	I _{ms} = 0 ma
I _f = 1.42 Amps ac	I ₁ = 0 ma
V _a = 607 volts	I ₂ = .6 ma
I _a = 3.4 ma	I _c = 3 ma
V _g = -10 volts	I _t = 4.4 ma
V _h = 1000 volts	Grid Mod. None

TABLE V (Continued)

INITIAL GUN OPERATING CONDITIONS FOR DATA

V_f = 9.25 vac	I_d = 0.60 ma
I_f = 1.48 amps ac	I_{ms} = 0 ma
V_a = 607 volts	I_1 = 0.05 ma
I_a = 1.73 ma	I_2 = 0.25 ma
V_g = -76 volts	I_c = 1 ma
V_h = 1000 volts	Grid Mod. Dial 84

2. Cold and Semi-Cold Tube Data

Three sets of microwave data were taken. These were for the following conditions:

- a. Cold tube - no beam, no plasma.
- b. Semi-cold tube - beam but no plasma.
- c. Hot tube - beam and plasma.

For each set of data, the following were determined: VSWR, transmitted signal, and radiated signal. In addition, the transmitted signal level relative to the radiated signal was calculated for the semi-cold and hot tube cases from the measured values for the transmitted and radiated signals.

The cold tube results are plotted in Figure 29. The transmitted signal, except for two points, was greater than 60 db down. On the basis of measuring instrument accuracy, it is estimated that the radiated signal data are accurate to within ± 1.5 db, the absolute frequency data to within ± 5 Mc. The frequency was estimated to be re-settable to within ± 1.5 Mc. Several features of Figure 29 are readily noticeable: (1) the radiated power oscillates wildly, at one point there is a change of 30 db in 10 Mc; (2) the average VSWR is high; and (3) the VSWR oscillates, but in a much smoother fashion than the radiated signal. Note that for VSWR's greater than three, the "actual" VSWR at the coupler may be considerably greater than that shown. This is because the attenuation in the cable between the bidirectional coupler and the coupler in the tube is about 1.4 db. The view taken here was to consider the performance of the device as that determined at the location of the test equipment. No attempt has been made to ascertain the performance as viewed at the couplers.

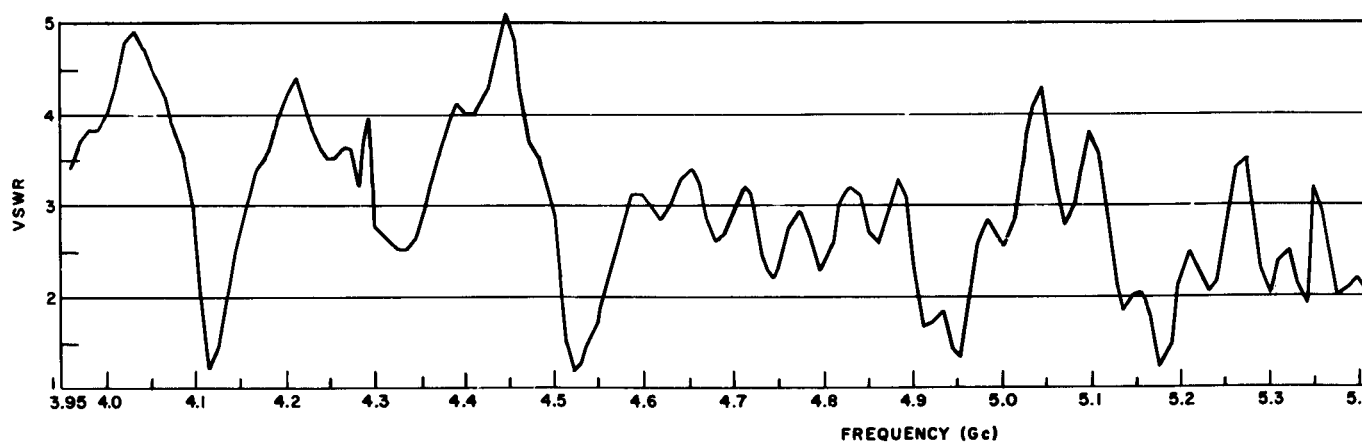
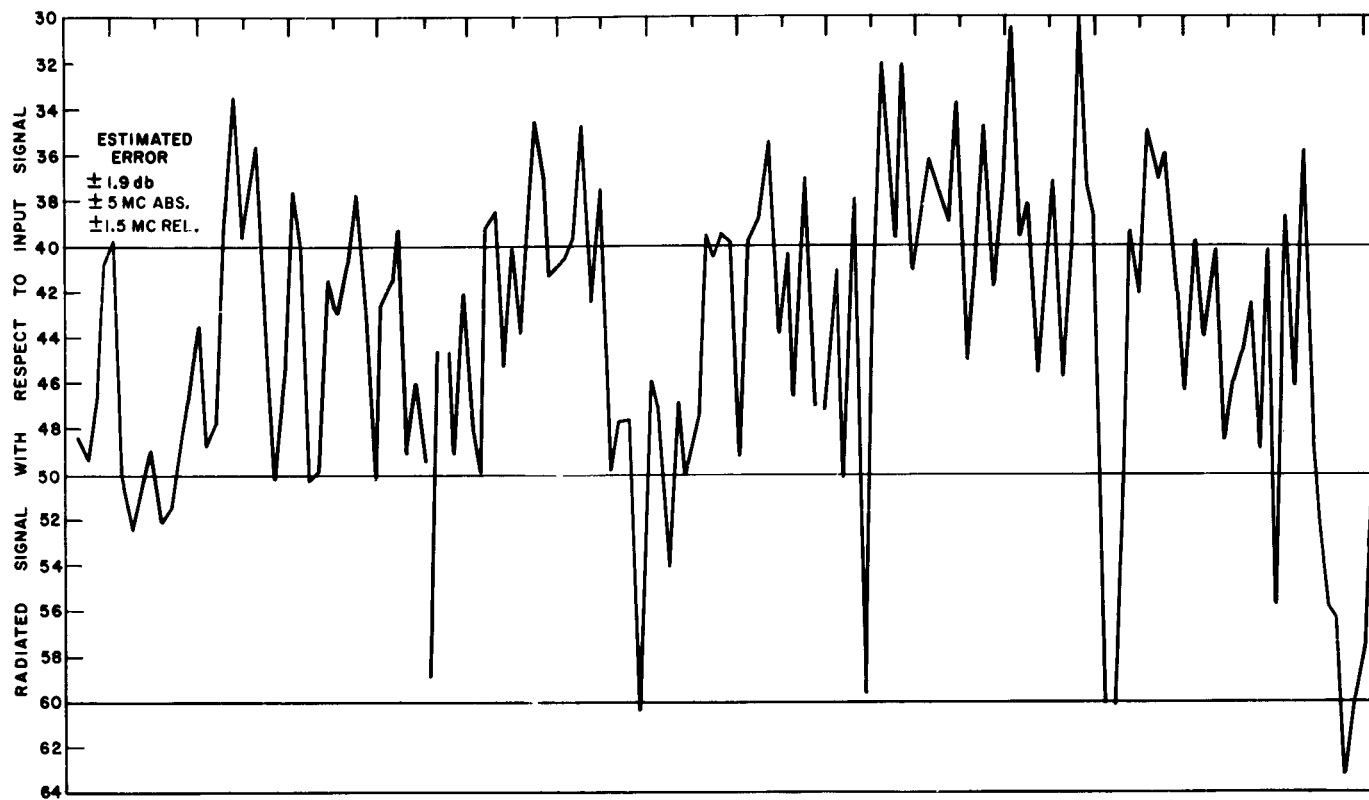
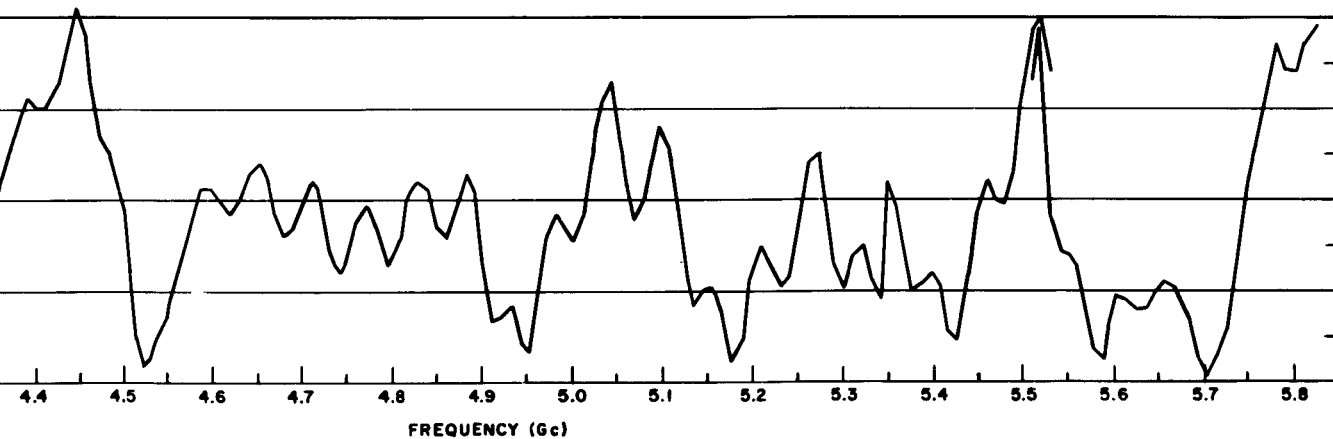
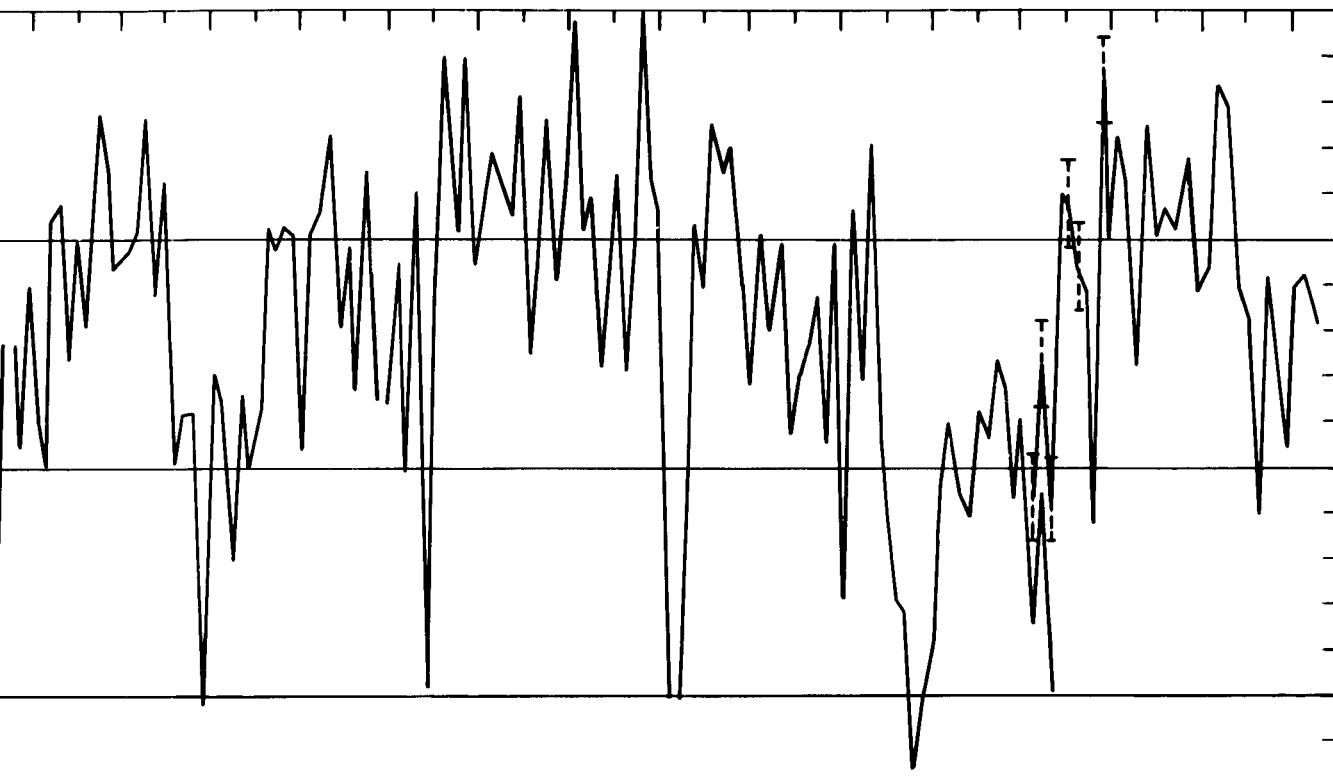


Figure 29. Cold Rel



2

Figure 29. Cold Tube VSWR and Radiated Signal
Relative to Input Signal

According to the best estimate, the radiation observed during the cold measurements is occurring directly from the input helix. The oscillations of radiated signal level as a function of frequency are most probably due to resonances in the helix and the cavity or cavities formed by the internal support structure and the vessel. There is no apparent correlation between the radiated signal level and the VSWR. Some problem was encountered in reproducing the data. Note the overlap curves at a frequency around 5.52 Gc. The reproduceability of the radiated signal is, from this one overlap, within 6 db. This overlap occurred as a result of taking data over a span of two days.

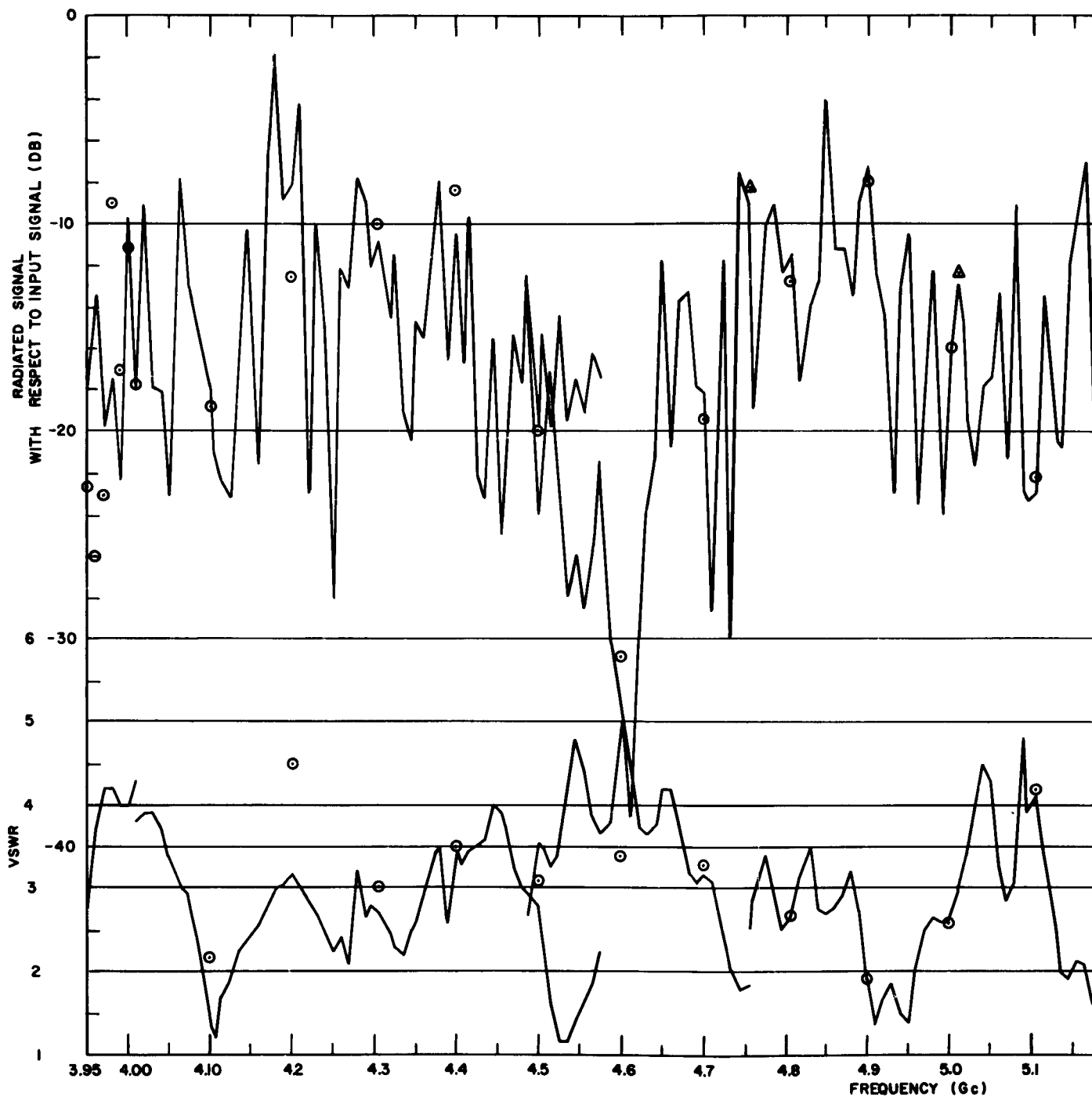
Results for the semi-cold measurements are shown in Figures 30, 31, and 32. Here the semi-cold tube VSWR, and radiated signal relative to input signal; the semi-cold tube transmitted signal relative to the input signal; and the transmitted signal relative to the radiated signal are plotted respectively. The data were taken over a span of three days, giving rise to three overlaps. Also plotted, as circled dots, are the results of a consistency check made on the third day at steps in frequency of 100 Mc. Again, oscillations are apparent in the radiated signal. Reproduceability of the radiated and transmitted signals is considered moderately good. On the other hand, reproduceability of the VSWR measurements is considered generally quite poor. The average radiated signal is 26 db above that of the cold tube. The most striking feature of these results for the semi-cold case is that the tube already exhibits gain for a significant fraction of the 1.9-Kmc bandwidth over which the measurements were made. This implies electronic gains of greater than 70 db. Again, there appears to be no obvious correlation between the various curves.

On the basis of the oscillations observed, one can conclude that unless the transmitted signal relative to the radiated signal changes drastically between the semi-cold and hot tube measurements, or a wide band effect occurs, a statistical analysis of the data will be required to ascertain whether there is significant enhancement of the radiation by the presence of a plasma.

Further, the fact that the average radiated signal relative to the transmitted signal for the semi-cold case is 26 db greater than the average radiated signal relative to the input signal for the cold case raises the question of whether the beam is radiating a signal in addition to that radiated by the couplers, and whether it is doing so with far greater efficiency.* There are at least four possible explanations for the observed discrepancy: These are:

- 1) The output coupler radiates with an efficiency of 26 db greater than that of the input coupler.
- 2) The heat shields and/or filaments, and/or end walls of the plasma region are effectively forming a cavity which the beam couples to and which, in turn, radiates.

* Noted added in proof: Measurements made since writing this report show that the output coupler is indeed a more efficient radiator by more than 12 db. This plus the higher power present on the output coupler might well account for this 26 db difference. This result also further justifies the use of the ratio of radiated to transmitted signal.



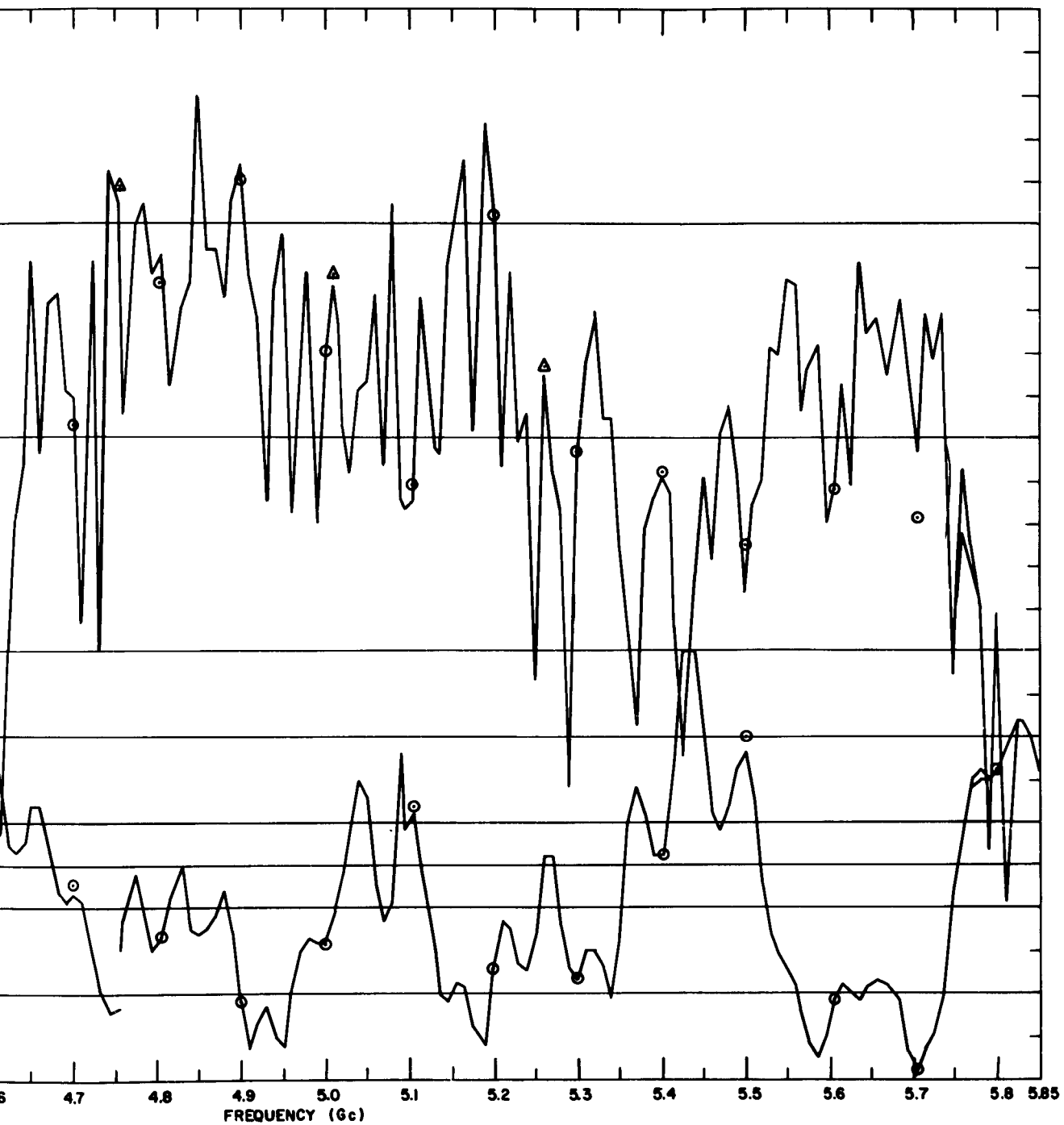
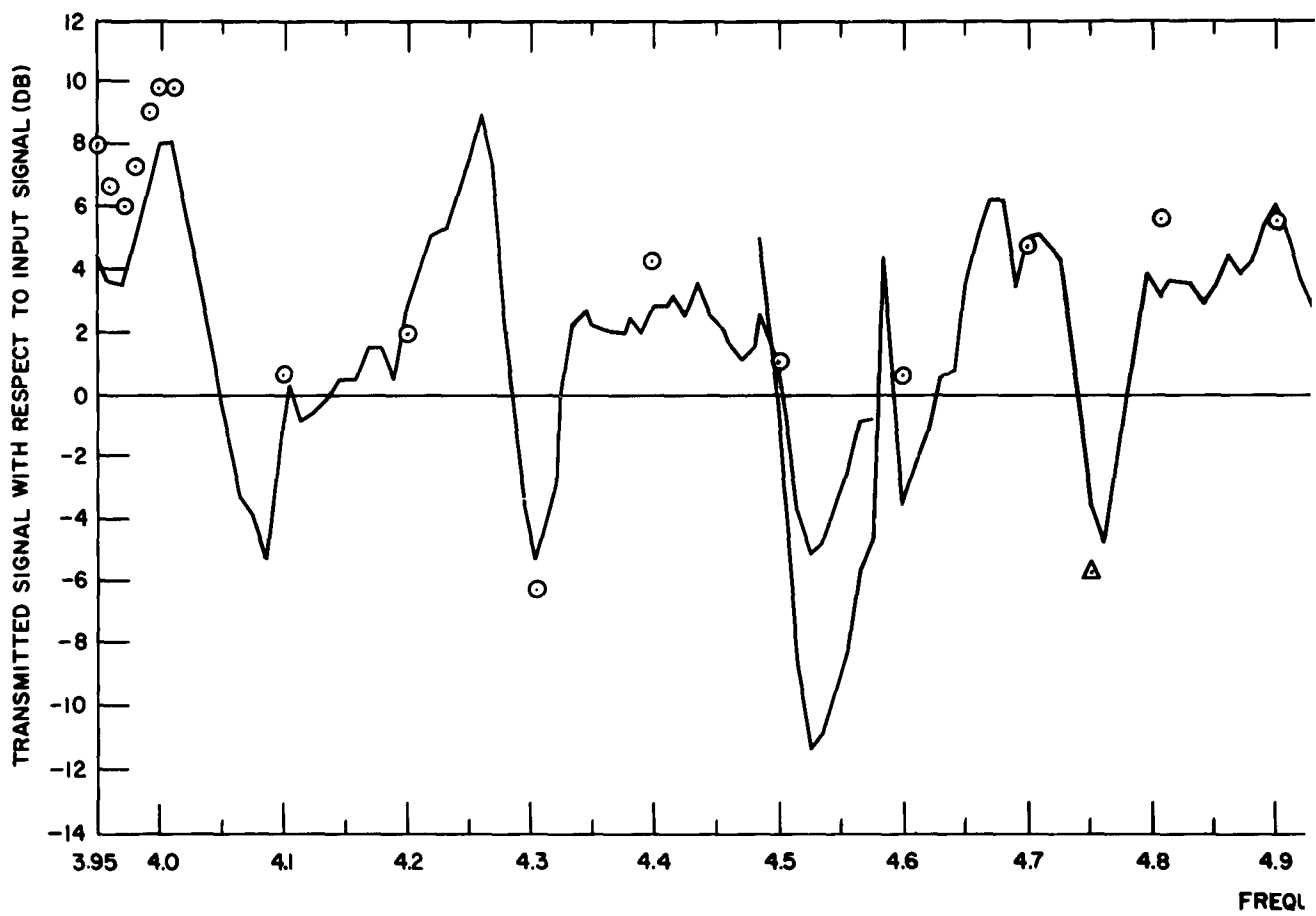
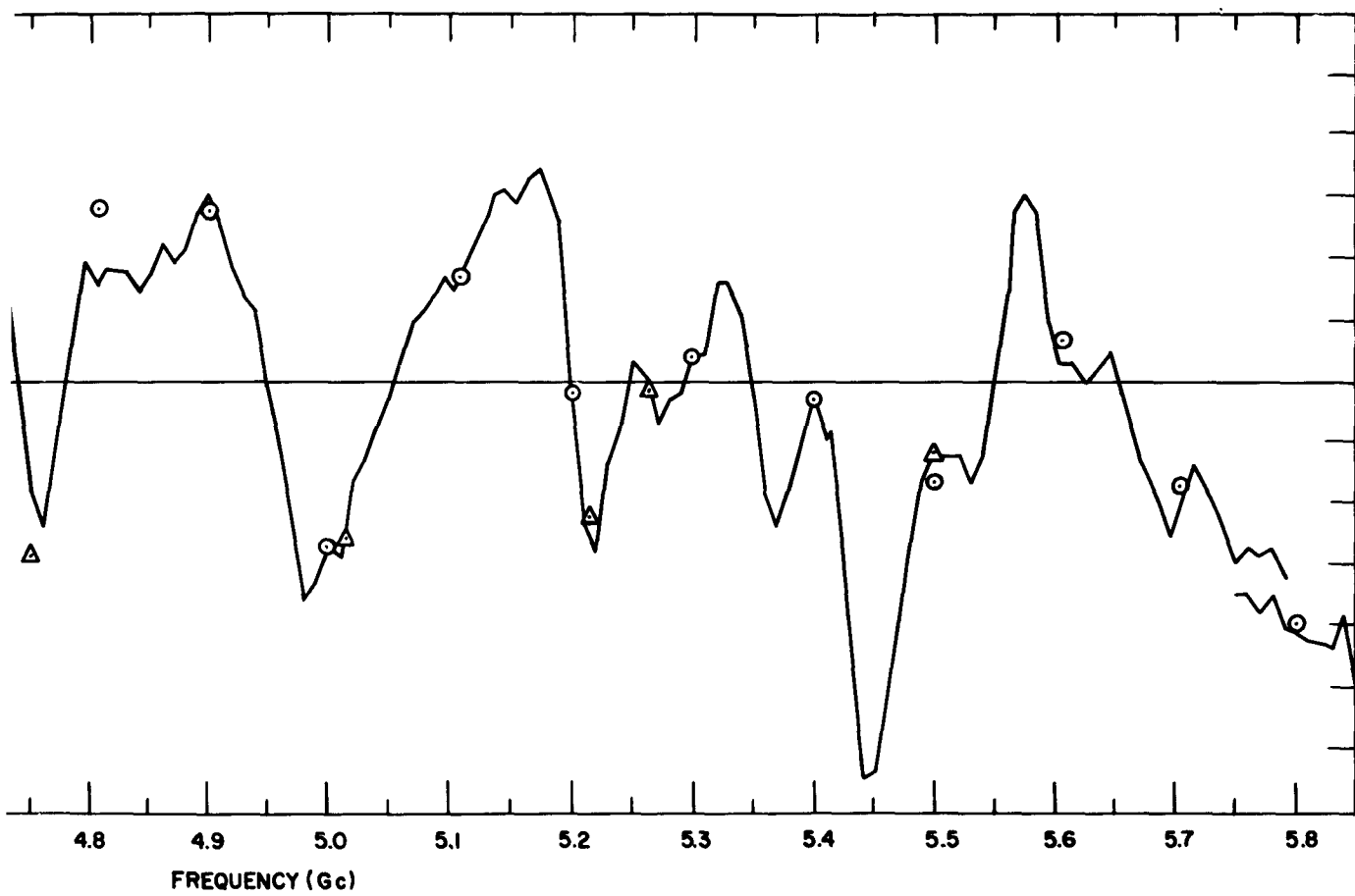


Figure 30. Semi-Cold Tube VSWR and Radiated Signal Relative to Input Signal

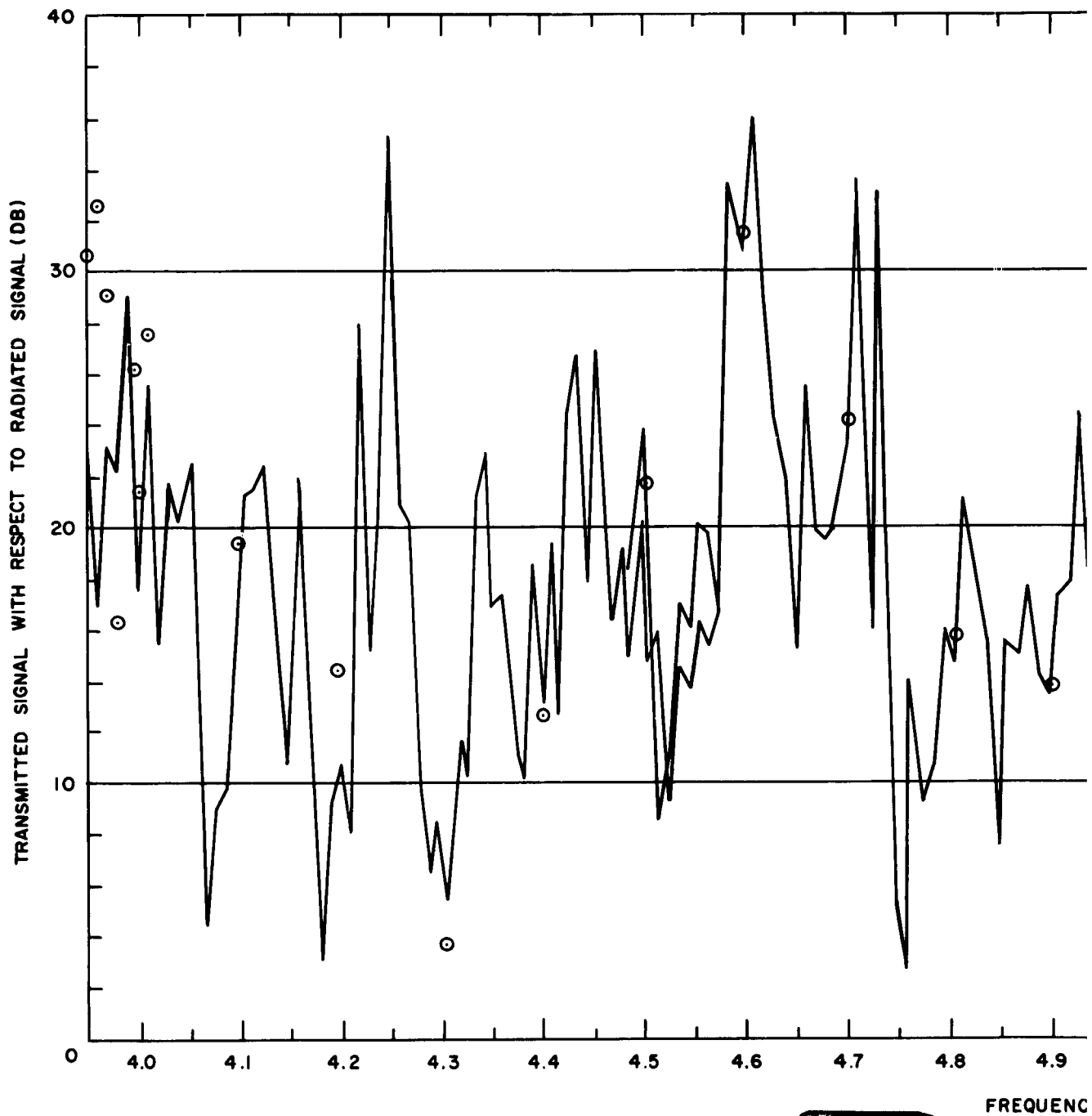
2

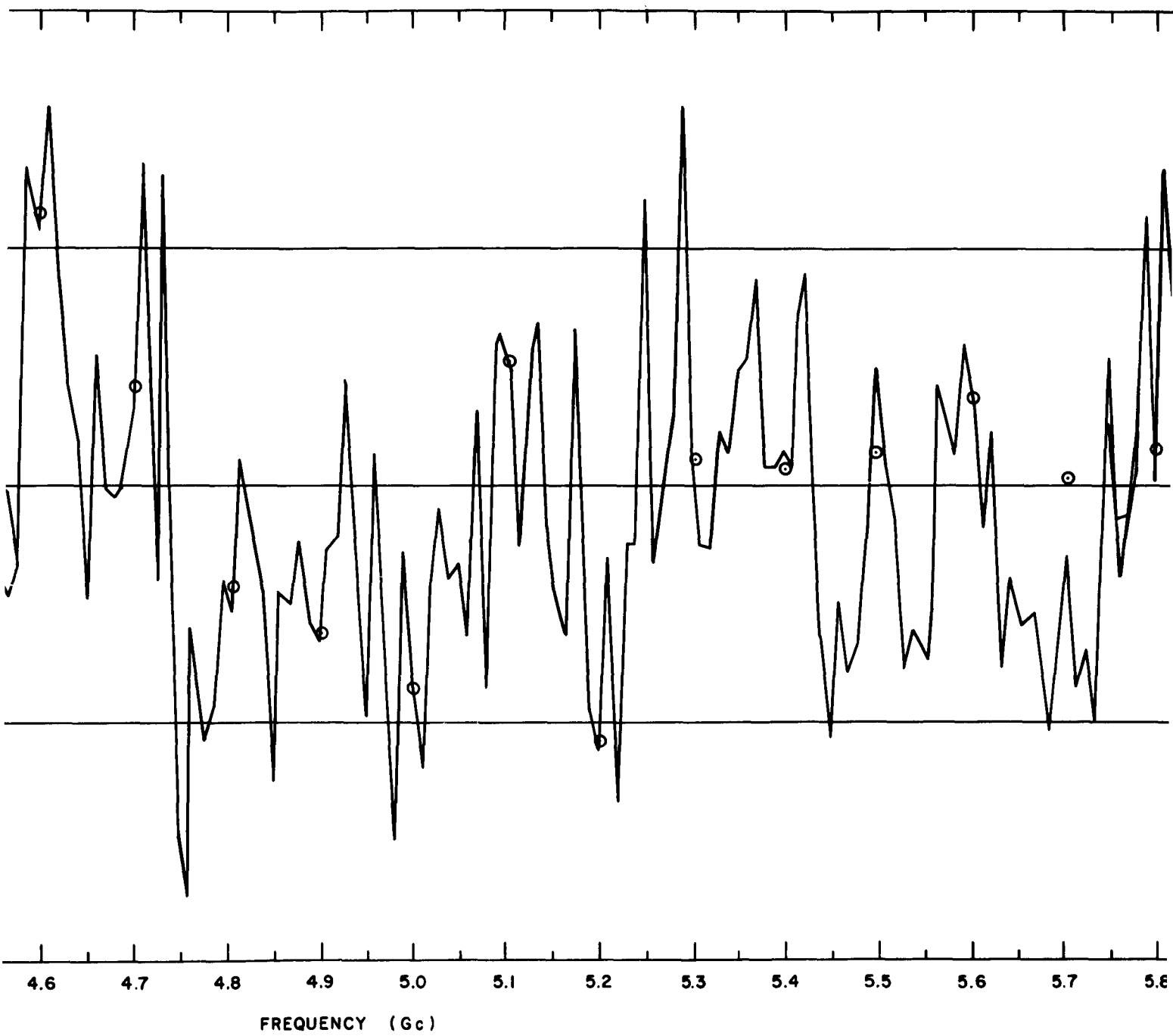




2

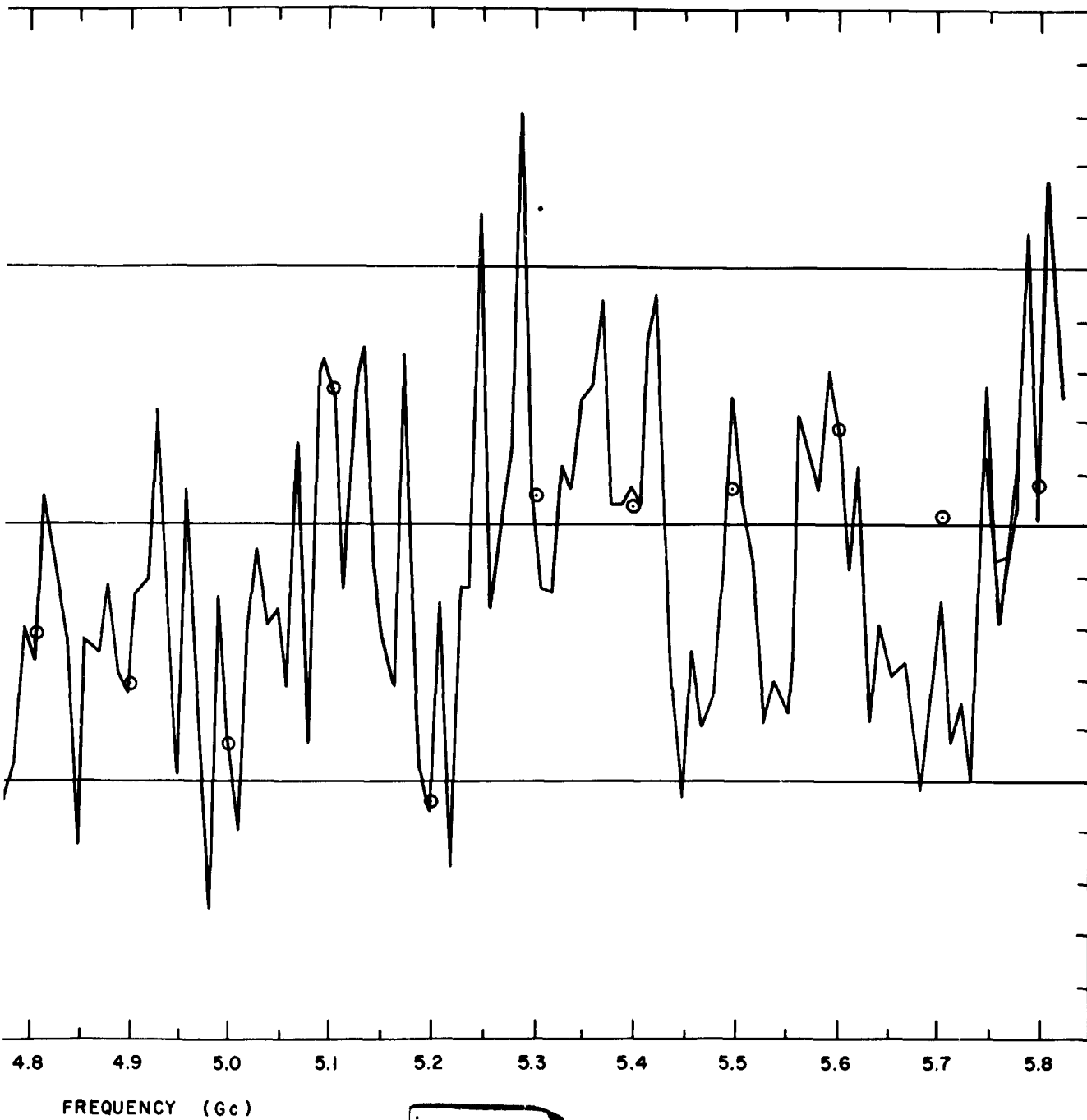
Figure 31. Semi-Cold Tube Transmitted Signal
Relative to Input Signal





2

Figure 32. Semi-Cold Tube Transmitted Sig
Relative to Radiated Signal



3

Figure 32. Semi-Cold Tube Transmitted Signal
Relative to Radiated Signal

- 3) The presence of the beam enhances the radiation efficiency of the helices.
- 4) The beam radiates.

The first explanation doesn't seem plausible. The second and third explanations are plausible. The last explanation is contrary to generally accepted theory if one assumes the beam to be infinitely long. However, the beam is, in effect, of finite length and is confined between two metal walls normal to it. Still, if explanation (4) is true, it represents a significant result. A set of experiments carefully designed to selectively eliminate various explanations is required to settle the question.

3. Hot Tube Data

Target operating conditions for the plasma are given in Table VI along with actual conditions. Clearly, the actual plasma conditions are far from the target figures. The measurement of the actual conditions is discussed in the last part of this section. The results of the hot tube measurements are plotted in Figures 33, 34, and 35. In Figure 33 the hot tube VSWR and radiated signal relative to the input signal are shown (red curves). In Figure 34 the transmitted signal relative to the radiated signal is shown and in Figure 35 is shown the transmitted signal power relative to the input signal power (i.e., the net gain curve). To facilitate comparison, the semi-cold data (black curves) are also shown in these figures. The error limits are the measured standard deviations. The methods of calculating the errors, and the rest of the statistical analysis, are discussed in Appendix V.

TABLE VI

TARGET AND ACTUAL PLASMA OPERATION CONDITIONS

Target Conditions

$f_c = 2.90 \text{ Gc}$	$f_h = 5.61 \text{ Gc}$
$B = 1.036 \text{ Kg}$	$T_{\text{res}} = 39.8^\circ \text{ C}$
$f_p = 4.8 \text{ Gc}$	% ionization = 90%
$n_e = 2.86 \times 10^{11} \text{ electrons/cm}^3$	$T_i = T_e \approx 1900^\circ \text{ K}$

TABLE VI (Continued)

TARGET AND ACTUAL PLASMA OPERATION CONDITIONS

Actual Conditions

$f_c = 2.90 \text{ Gc}$	$f_h < 3.2 \text{ Gc}$
$B = 1.036 \pm 10 \text{ Kg}$	$T_{\text{res}} = 39.7^\circ \text{ C}$
$f_p < 1.3 \text{ Gc}$	% ionization = unknown
$n_e < 2.2 \times 10^{10} \text{ electrons/cm}^3$	$T_i \approx T_e < 1830^\circ \text{ K}$

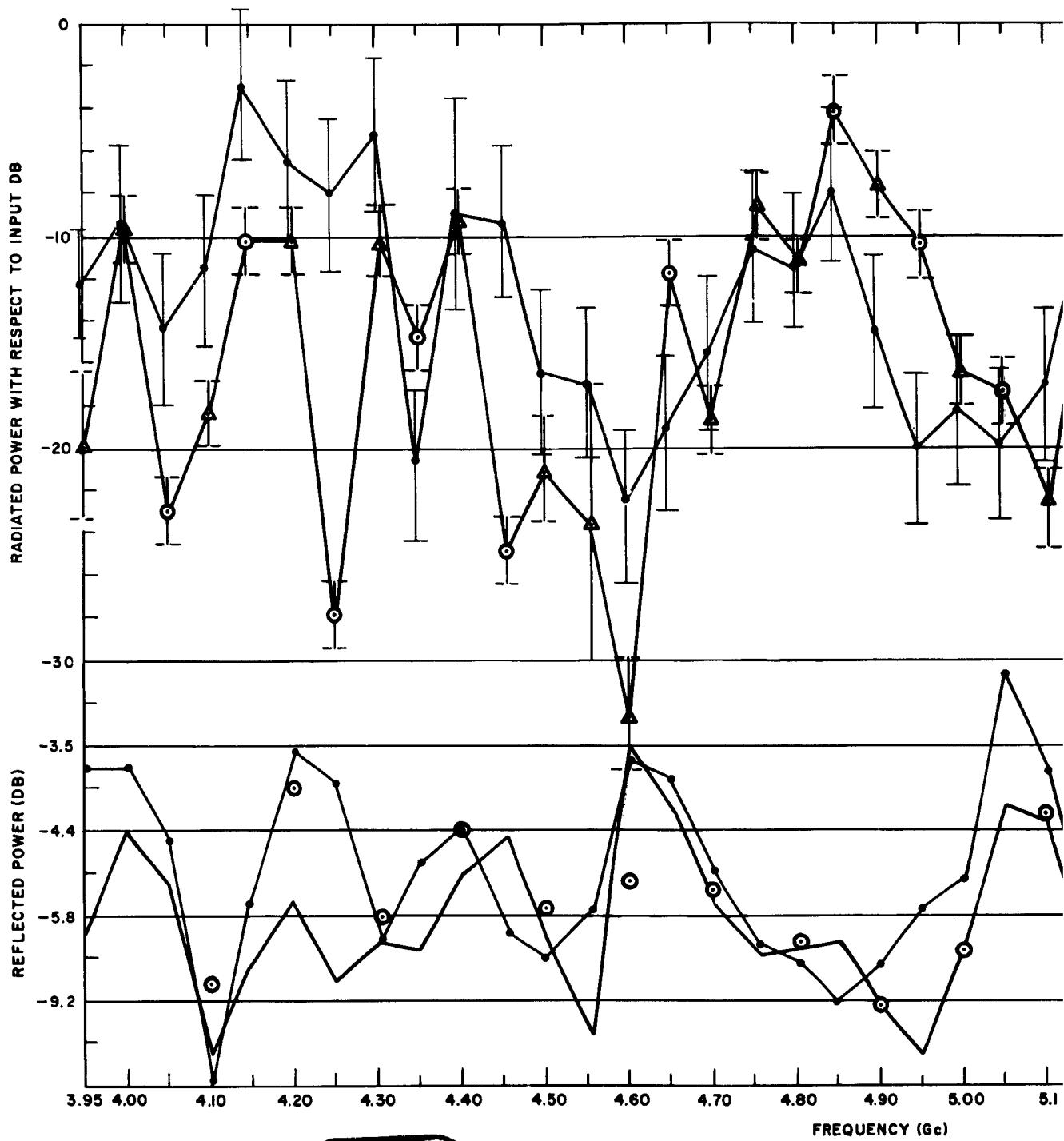
Examination of the curves leads to several important tentative conclusions:

- 1) The presence of the plasma significantly enhances the radiation at some frequencies (Figure 34).
- 2) In general there is little change in net gain due to the presence of the plasma (Figure 35).
- 3) From 1 and 2 it follows that the plasma under certain conditions is apparently acting as an impedance match between the beam and free space.
- 4) There is no obvious consistent correlation between the VSWR curve and the other curves.

A detailed statistical analysis of the data confirms these tentative conclusions. The chi-square test shows that there is less than .5% chance that the hot tube curves of Figures 33 and 34 are the same as the semi-cold tube curves. Further, in Table VII we have tabulated the most statistically significant points of change by the plasma for the radiated relative to transmitted signal. These points were determined by the t-test. Also, the significant points for the other two quantities have been tabulated.

An examination of Table VII suggests the following tentative conclusions. An increase in radiated-vs-transmitted signal is accompanied by an increase in radiated-vs-input signal, and by either no change or a decrease in gain.

These results are both surprising and encouraging. We had expected to see little effect in the region investigated (i.e., $f > f_h = \sqrt{f_p^2 + f_c^2}$), but we find an effect of significant magnitude at points in this region.



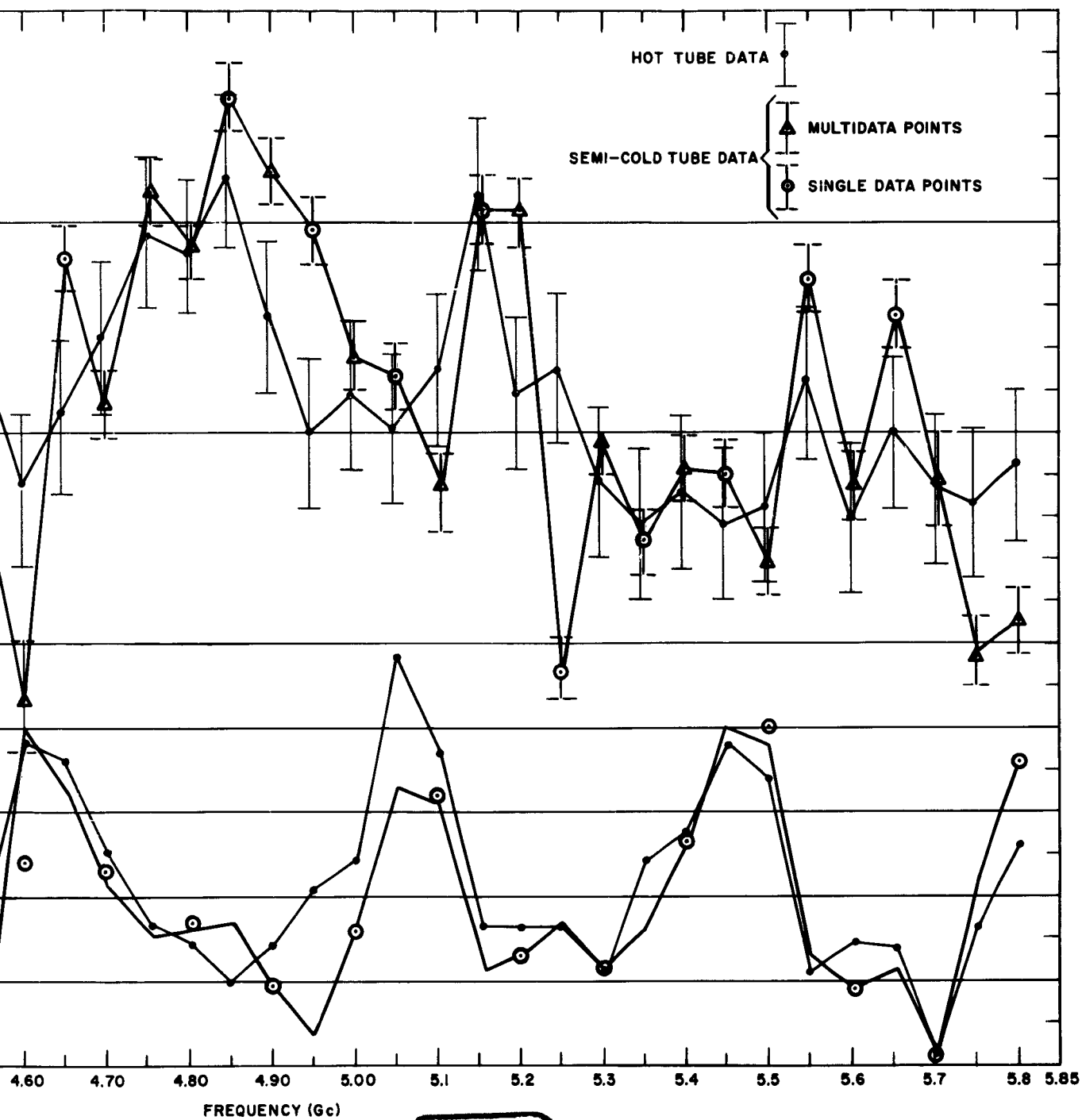
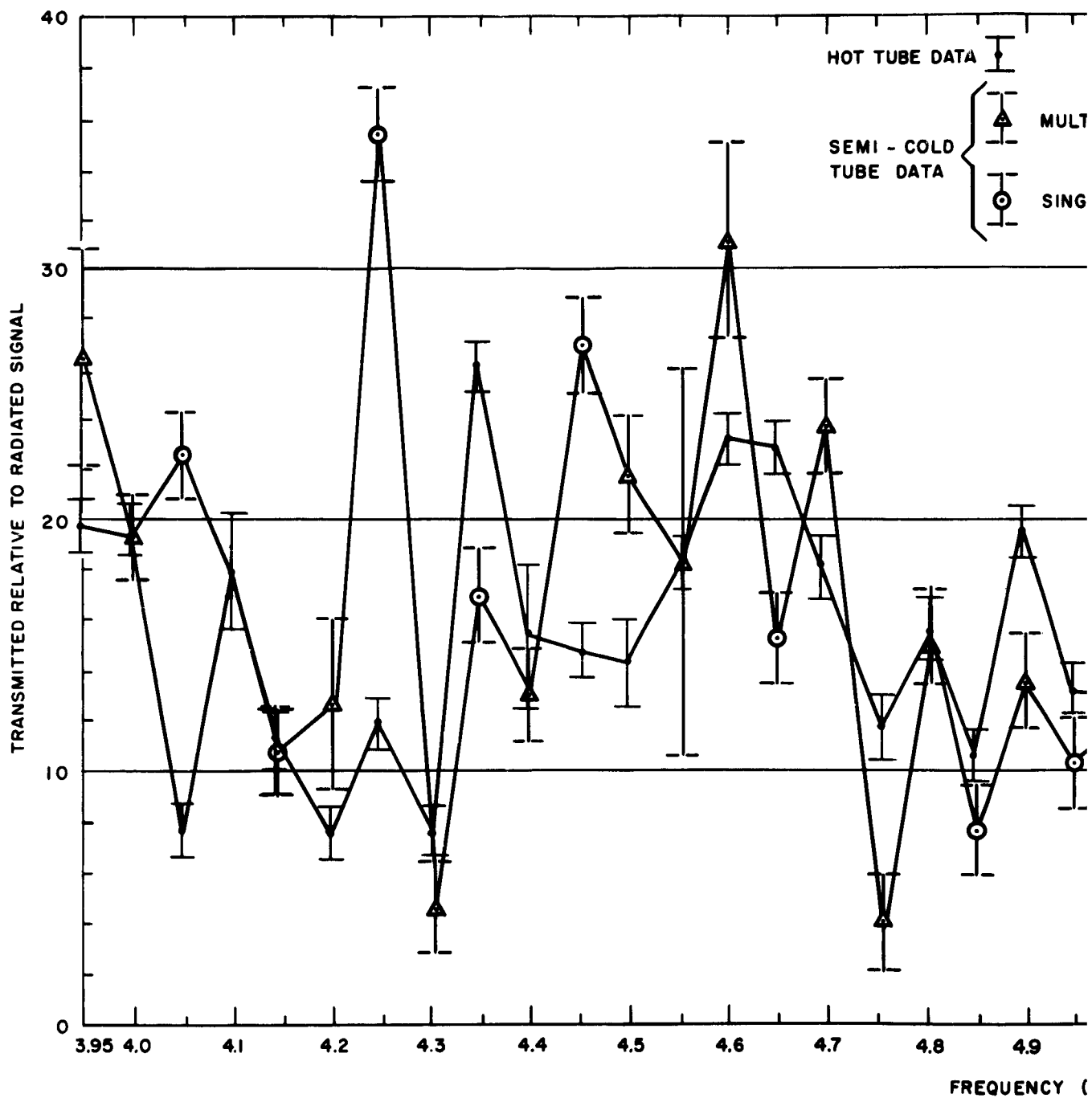
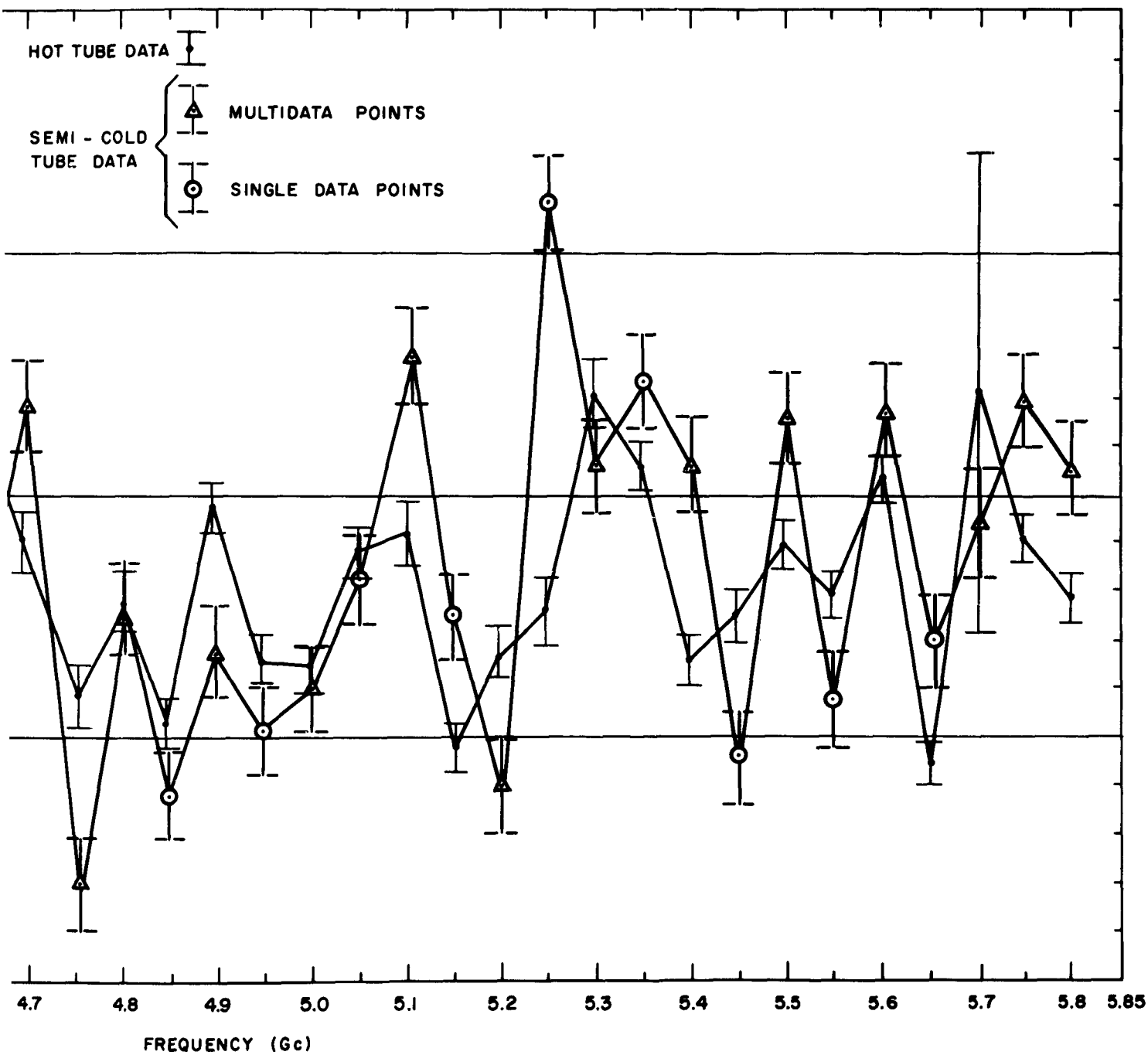


Figure 33. Hot Tube VSWR and Radiated Signal Relative to Input Signal

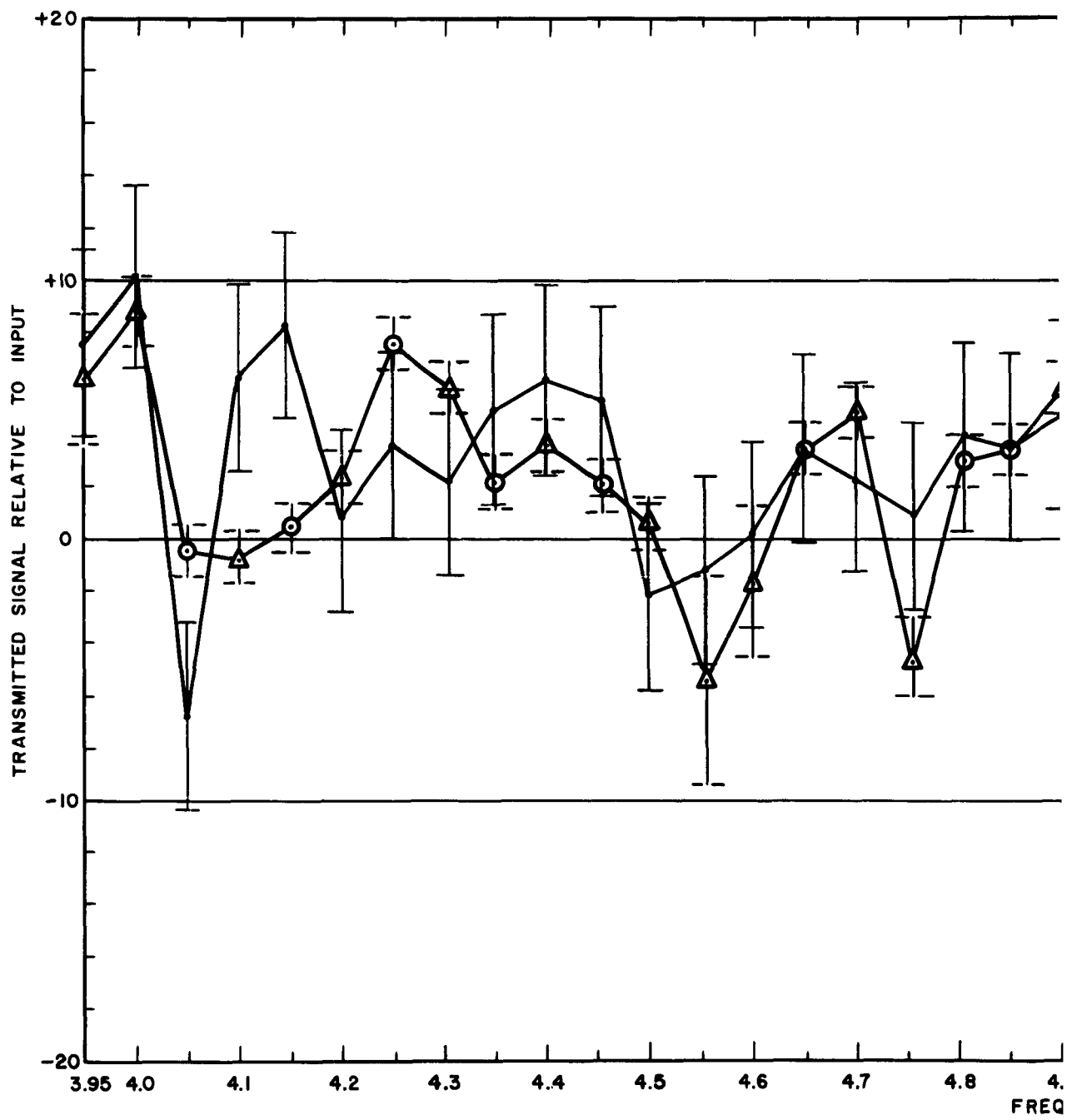
2





2

Figure 34. Hot Tube Transmitted Signal Relative to Radiated Signal



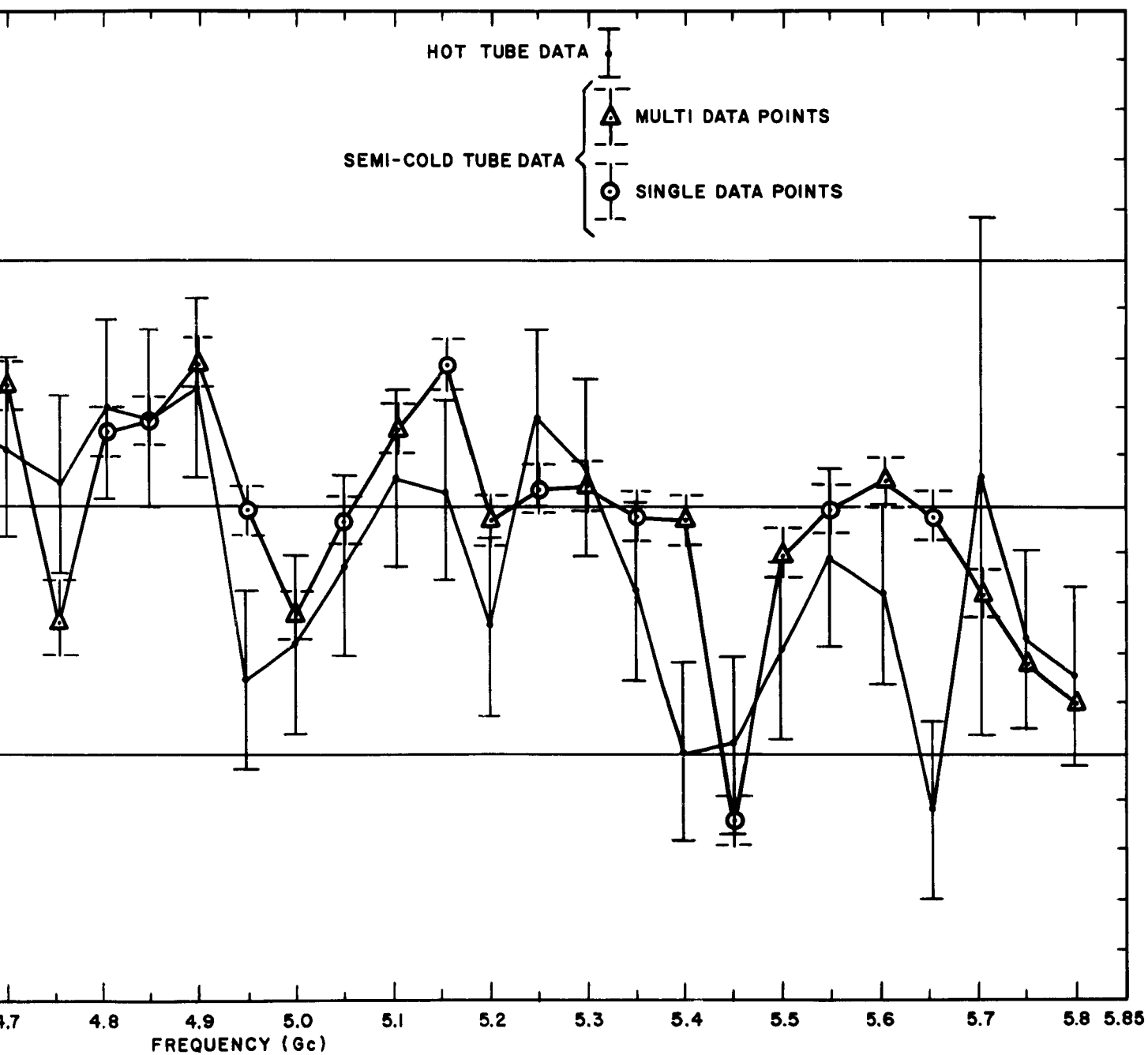


Figure 35. Hot Tube Transmitted Signal Relative to Input Signal

2

TABLE VII
SIGNIFICANT POINTS OF PLASMA EFFECT ON RADIATION

Frequency (GC)	Radiated Signal-vs-Transmitted Signal		Radiated Signal-vs-Input Signal		Transmitted Signal-vs-Input Signal	
	Difference (Increase) [DB]	Significance (Probability due to chance)	Difference (Increase) [DB]	Significance (Probability due to chance)	Difference (Increase) [DB]	Significance (Probability due to chance)
3.95			8.1	.2-.1		
4.05	15.05	.1-.05	8.6	.2-.1	-6.45	.4-.3
4.25	23.4	.05-.02	19.8	.2-.1		
4.305	-2.95	.2-.1	5.15	.3-.2		
4.35	-8.9	.1-.05	-6.15	.3-.2		
4.455	12.3	.1-.05	15.5	.2-.1		
4.5	7.55	.2-.1				
4.6			9.8	.2-.1		
4.65	-7.5	.2-.1	-7.5	.3-.2		
4.7	5.65	.1-.05				
4.755	-7.52	.2-.1			4.48	.6-.5
4.9	-5.9	.02-.01	-6.9	.3-.2		
5.105	7.25	.2-.1	5.4	.3		
5.155	5.7	.2-.1			-5.0	.4-.3
5.2	-5.4	.1-.05	-8.65	.2-.1		
5.25	+17	.02-.01	14.3	.2-.1		
5.40	8.2	.05-.02			-9.35	.2-.1
5.45	-5.7	.2-.1				
5.50	5.4	.2-.1				
5.605	2.9	.1-.05				
5.655	5.1	.2-.1	-6.7	.3-.2	-10.8	.2-.1
5.75	5.8	.2-.1	6.9	.3-.2		
5.80	5.35	.05-.02	6.5	.3-.2		

B. PLASMA

Measurements of the plasma were carried out using the instrumentation described in Section IV, B-2. The method of analysis of the double probe trace is that given by E. O. Johnson and L. Malter¹⁰. To calculate the plasma density from the probe curves, the ion temperature was taken to be equal to the electron temperature. This is a reasonable assumption if the plasma is truly quiescent. The resulting limits on plasma density and temperature have been given in Table VI.

We have not, as yet, found a satisfactory explanation for the discrepancy between the target and the observed plasma densities. Possible explanations include:

- 1) Considerably higher leak rate for cesium gas from the region inside the quartz tube than anticipated.
- 2) Lower ionization efficiency by the filaments than anticipated.

Without measurements of the neutral cesium density it is very difficult, if not impossible, to find a totally satisfactory explanation.

A number of difficulties were encountered with the instrumentation. Further, some unexpected phenomena were encountered. Pickup of the 400-cycle heating-current pulses was observed on the oscilloscope traces. This was apparently due in part to poor common mode rejection. (The scope technique suffers from poor common mode rejection when using the P6000 probes.) Although this can be corrected by the use of precision attenuators instead of probes, it had not been anticipated as serious problem prior to the performance of the experiments on the basis of results from tests with a dummy load. When the X-Y recorder was used, asymmetrical hysteresis curves were encountered. Further, indications of a strong density gradient were found.* Finally, the outer (Beryllia) insulator on the double probe broke after making measurements at only one point (near the beam). This terminated the measurements prematurely.

The combined effect of the above difficulties prevented us from obtaining enough good data on the plasma to make a determination of the plasma properties better than the results given in Table VI.

*The density gradients provide complications which can be eliminated by going to a two-parallel-wire geometry for the probe.

SECTION VI

CONCLUSIONS AND RECOMMENDATIONS

A. CONCLUSIONS

An experiment was performed to detect coherent radiation by plasma oscillations stimulated by a modulated electron beam. From the results of this experiment it is concluded that:

1. Enhancement of the radiation by the presence of a plasma has been positively identified. (Electronic gains as great as 23 db for the radiated signal were observed.)
2. The radiation gains in the region above the hybrid frequency show a resonant-like behavior with resonant half widths in general, less than 100 mc.
3. Generally, no change in the straight-through (transmitted signal) gain was observed.
4. Results definitely indicate that the work should be extended to other regions of relative frequency. The effects of the various parameters should be further investigated.

B. RECOMMENDATIONS FOR FUTURE WORK

It is recommended that the following three sets of experiments be carried out as the next step in:

1. An additional search for radiation at frequencies below 1.25 times the hybrid frequency. Particular attention should be paid to the region between the cyclotron and the hybrid frequencies since theory suggests that the radiated power should be strongest in this region.
2. Experiments at higher modulation powers and beam powers to investigate possible saturation effects. If such saturation effects exist they could seriously limit the power capabilities of beam plasma devices. This is a class of experiments which appears to have been neglected up to this point by the workers in the field.
3. Further investigations of the effects of beam voltage.

In order to conduct these experiments, it will be necessary to make some modifications in the facility and to carry out some supporting experiments.

REFERENCES

1. D. Bohm and E. P. Gross, "Theory of Plasma Oscillations: A. Origin of Medium Like Behavior," Phys Rev 25, 1851-1864 (1949).
2. D. Bohm and E. P. Gross, "Theory of Plasma Oscillations: B. Excitation and Damping of Oscillations," Phys Rev 75, 1964-1875 (1949).
3. D. Bohm and E. P. Gross, "Effects of Plasma Boundaries in Plasma Oscillations," Phys Rev 79, 992-1001 (1950).
4. G. D. Boyd, Experiments on the Interaction of a Modulated Electron Beam with a Plasma, California Institute of Technology, Electron Tube and Microwave Laboratory, Technical Report No. 11, AD-218991 (May, 1951).
5. L. M. Field and R. W. Gould, Quarterly Status Report No. 17, April 1, 1957 to June 30, 1957 Vacuum Tube Research Project, California Institute of Technology, AD-2003697 (1957). Also see other quarterly status reports on this project.
6. M. A. Allen and G. Kino, "Interaction of an Electron Beam with a Fully Ionized Plasma," Phys Rev Letter, 6 163-165 (Feb. 5, 1961).
7. G. S. Kino, "Millimeter Wave Generation and Amplification in Plasmas," Paper No. XVII, Symposium on Solid State and Plasma Physics, Johns Hopkins University, November 3-4, 1959, Radiation Laboratory Report No. AF-13(1959).
8. R. E. Skinner, "Beam-Plasma and E. M. Wave Plasma Interactions for Microwave Generation - A Review," (unpublished) (see, also, proposal for this contract).
9. R. C. Knechtli and J. Y. Wada, "Generation and Measurement of Highly Ionized Quiescent Plasmas in Steady State" Phys Rev Letters 6, No. 5, 215-217 (March 1, 1962).
10. E. O. Johnson and L. Mather, "A Floating Double Probe Method for Measurements in Gas Discharges" Phys Rev 80, No. 1, 58-68 (October 1, 1950).
11. R. L. Colby and R. E. Skinner, "Design of Large Air Core Magnets for Plasma Physics Research," Company Correspondence (June, 1961).
12. Carl A. Bennett and Norman L. Franklin "Statistical Analysis in Chemistry and the Chemical Industry" John Wiley and Sons, Inc., New York, 177 (1954).
13. Harold Cramer, "Mathematical Methods of Statistics" Princeton University Press, Princeton, 416-452 (1946).

APPENDIX I

MAGNET DESIGN

The problem of designing a magnet such as that used in the POD machine is a formidable one and requires the use of high speed computers. The over-all problem can be broken down into two sub-problems. The first of these is to determine the magnet geometry and/or current distribution required to give the desired field configuration. The second sub-problem then becomes that of determining conductor, insulation, power supply, and cooling system requirements, and to do this within the constraint that the over-all system configuration be a practical one.

To carry out the requisite calculations, three FORTRAN codes were written for the IBM 7090 computer. These were:

1. MAG FIELD I: — calculates normalized field along the axis of a single multilayer air-core solenoid.
2. MAG FIELD II: — calculates the normalized field along the axis for two identical multilayer air core solenoids separated by a gap.
3. SOL COOLING I — determines the cooling system characteristics given the magnet geometry, allowable conductor size, insulation thickness, and power supply characteristics.

The first code was written to give us some feel for the field of a single multilayer solenoid. The results did not help us as much as had been hoped. All of the calculations were based upon earlier work done by us for another program ¹².

The geometry for the magnetic field calculations is shown in Figure 36. The field from such magnets is given by the following equation:

$$B = 2\pi \times 10^{-1} \text{ j a}^2 G(\alpha_1, \alpha_2, \alpha_3, \alpha_7)$$

where the quantity G is a function of dimensionless parameters and is dependent only upon the geometry. The dimensionless parameters in terms of the basic geometric dimensions of Figure 36 are:

$$\alpha_1 = b/a$$

$$\alpha_2 = c/a$$

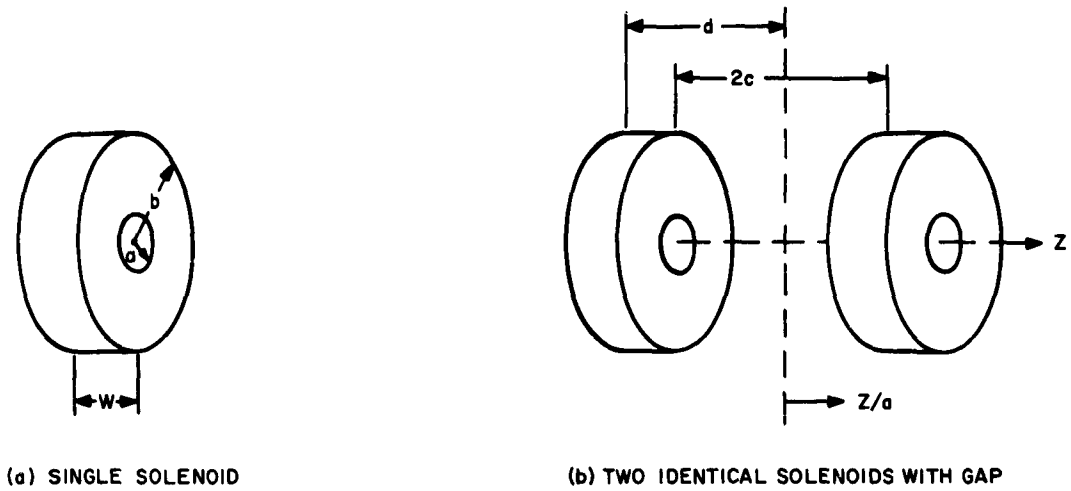


Figure 36. Geometry for Magnetic Field Calculations

$$\alpha_3 = d/a$$

$$\alpha_7 = w/a \text{ and}$$

$$\alpha = z/a$$

For a single layer solenoid it is easily shown that G is given by

$$G = \alpha_7 \left\{ \alpha \log \left[\left(\alpha_1 + \sqrt{\alpha_1^2 + \alpha^2} \right) / \left(1 + \sqrt{1 + \alpha^2} \right) \right] \right. \\ \left. + (\alpha_7 - \alpha) \log \left[\left(\alpha_1 + \sqrt{\alpha_1^2 + (\alpha_7 - \alpha)^2} \right) / \left(1 + \sqrt{1 + (\alpha_7 - \alpha)^2} \right) \right] \right\}$$

where α is the normalized distance from one end of the solenoid and is taken to be positive in the direction going into the magnet. This is the basic equation of the MAG

FIELD I code. For two identical solenoids with a gap, G is given by

$$G = \alpha_7 \left\{ (\alpha_3 - \alpha) \log \left[\frac{(\alpha_1 + \sqrt{\alpha_1^2 + (\alpha_3 - \alpha)^2})}{(1 + \sqrt{1 + (\alpha_3 - \alpha)^2})} \right] \right. \\ + (\alpha - \alpha_2) \log \left[\frac{(\alpha_1 + \sqrt{\alpha_1^2 + (\alpha_2 - \alpha)^2})}{(1 + \sqrt{1 + (\alpha_2 - \alpha)^2})} \right] \\ - (\alpha_2 + \alpha) \log \left[\frac{(\alpha_1 + \sqrt{\alpha_1^2 + (\alpha_2 + \alpha)^2})}{(1 + \sqrt{1 + (\alpha_2 + \alpha)^2})} \right] \\ \left. + (\alpha_3 + \alpha) \log \left[\frac{(\alpha_1 + \sqrt{\alpha_1^2 + (\alpha_3 + \alpha)^2})}{(1 + \sqrt{1 + (\alpha_3 + \alpha)^2})} \right] \right\}$$

where α is now the distance along the axis measured from the center of the gap. This is the basic equation of the MAG FIELD II code. A large number of survey calculations were made using the MAG FIELD II code. The most promising region was chosen and detailed calculations were made. Plots of normalized magnetic field as a function of α for $\alpha_2 = 0.5$, $\alpha_3 = 1.2$, and for three values of α_1 are shown in Figure 37.

Having chosen the approximate values for the geometrical parameters, it is necessary to determine the conductor dimensions, the voltage drop across the magnet and the current through the magnet required to give the desired field, and the requisite coolant flow rate and pressure drop required to keep the coolant temperature rise within the desired limits (outlet temperature less than 80° C). One is given the conductivity of the conductor, σ ; the insulation thickness; the density of the coolant, ρ ; the kinematic viscosity of the coolant, η ; specific heat of the coolant, c ; the thermal conductivity of the conductor; the coolant inlet temperature; the allowable coolant temperature rise, ΔT_1 ; the allowable pressure drop along the coolant channel; the set of allowable values of conductor size and coolant channel diameter, D ; allowable values of inside radius; α_1 , α_2 , and α_3 ; and the desired value of the magnetic field.

New values of α_1 and α_3 are later calculated by the code to satisfy the constraint that the number of turns in a single layer spiral winding be an integer, and that the number of pancake coils be an even integer. The basic equations for the calculations performed by the code are:

$$I = t_3^2 j$$

and

$$j = B \left[2\pi \times 10^{-1} a^2 G(\alpha : \alpha_1, \alpha_2, \alpha_3, \alpha_7) \right]^{-1}$$

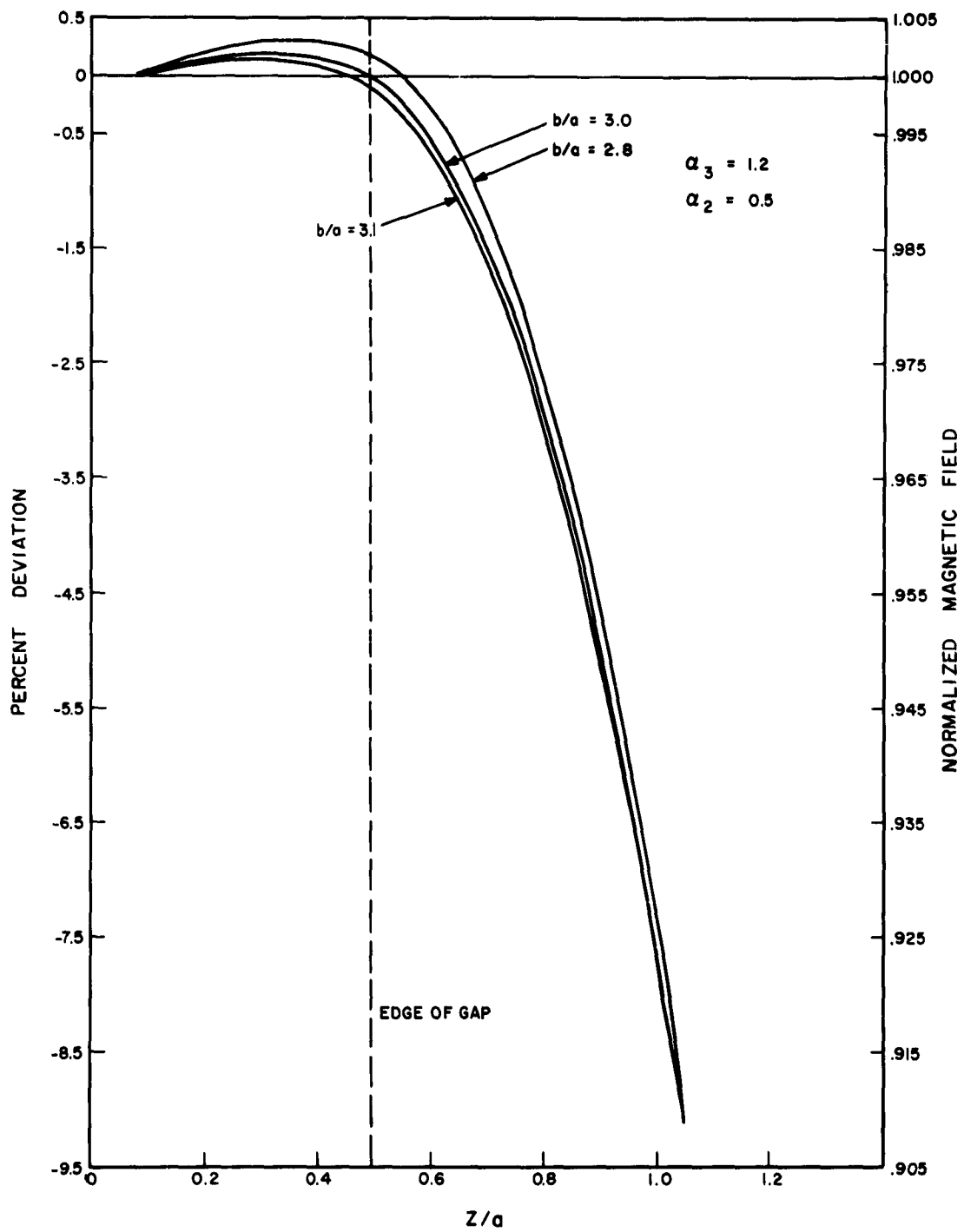


Figure 37. Calculated Normalized Magnetic Field Plot with α_1 as the Parameter

where I is the current through the magnet and t_3 is the thickness of the conductor plus twice the insulation thickness (i.e., t_3^2 is the area of a basic conductor cell). The total resistance of a pancake coil is given by

$$R = 2 \ell / (A_2 \sigma)$$

where ℓ is the total conductor length in a pancake coil and A_2 is the cross-sectional area of the conductor proper. The power, P_s , in a pancake coil is then

$$P_s = I^2 R$$

It then can be shown that for turbulent flow, the pressure drop through a pancake coil is given by

$$p = 2(0.046) \ell \left[4P_s / s\pi (\Delta T)_1 c \right]^{1.8} \eta^{0.2} / \rho D^{4.8}.$$

where s is Joule's constant and D is the diameter of the coolant channel.

For purposes of the code, this last equation has been inverted and combined with some of the other relationships to give the coolant channel diameter and conductor dimensions in terms of p and the other parameters and physical constants. These are then compared with the values of allowable conductor dimensions, previously specified, and the closest set of allowable values are chosen. Then the calculation is inverted to give the maximum field, voltage drop through the magnet, the resistance of the magnet, the current through the magnet, the coolant flow rate, the coolant temperature rise, etc. The calculated results for the magnet actually built are given in Table VIII.

TABLE VIII

CALCULATED MAGNET PARAMETERS

$\alpha_1 = 2.6$	$\alpha_2 = 0.5$
$\alpha_3 = 1.1$	$\alpha_7 = 0.6$
$a = 7$ in	$b = 18.2$ in
$c = 3.5$ in	$t_1 = 0.270$ in
$t_2 = 0.015$ in	$W = 4.2$ in

TABLE VIII (Continued)

CALCULATED MAGNET PARAMETERS

B = 3.57 gauss	p = 85 psi
l = 492 ft	I = 229 amps
V = 333 volts	ν = 5.79 gal/min
P = 76.4 kw	T _{in} = 30 °C
T _{out} = 80 °C	

The discrepancy between the calculated and actual values rises from the fact that the magnet design was fixed in final form before the vacuum vessel design was complete; it was later found necessary to increase the gap dimensions from 7.000 inches to 7.375 inches.

APPENDIX II

MAGNET SUPPLY CIRCUIT

The magnet supply is shown in Figure 38 and the magnet supply circuit diagram is shown in Figure 39. The capability of the power supply can be increased by a factor of 1.3 by the addition of another variac and appropriate current balancing chokes. It will also probably be necessary, if this is done, to replace the silicon diode rectifiers with larger units. The variacs are driven by a 7:1 reduction ratio chain drive.

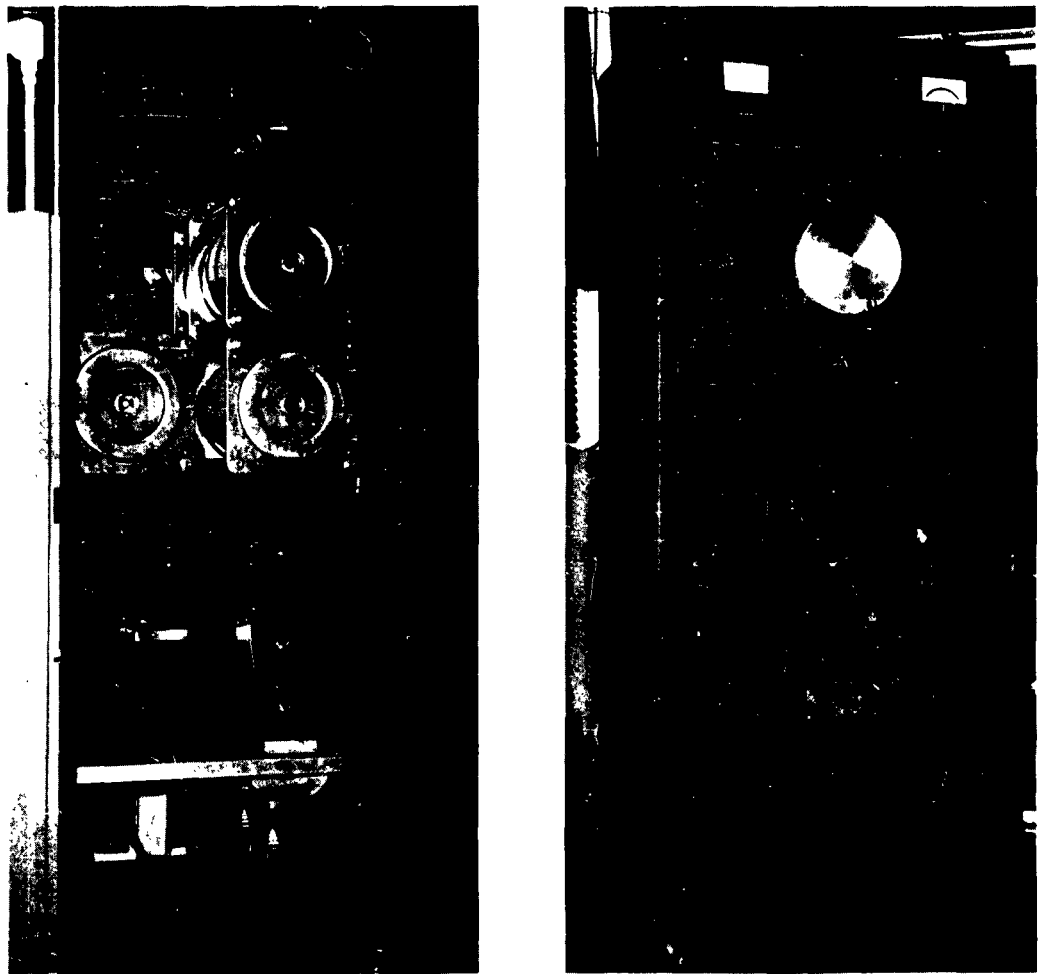


Figure 38. Magnet Supply

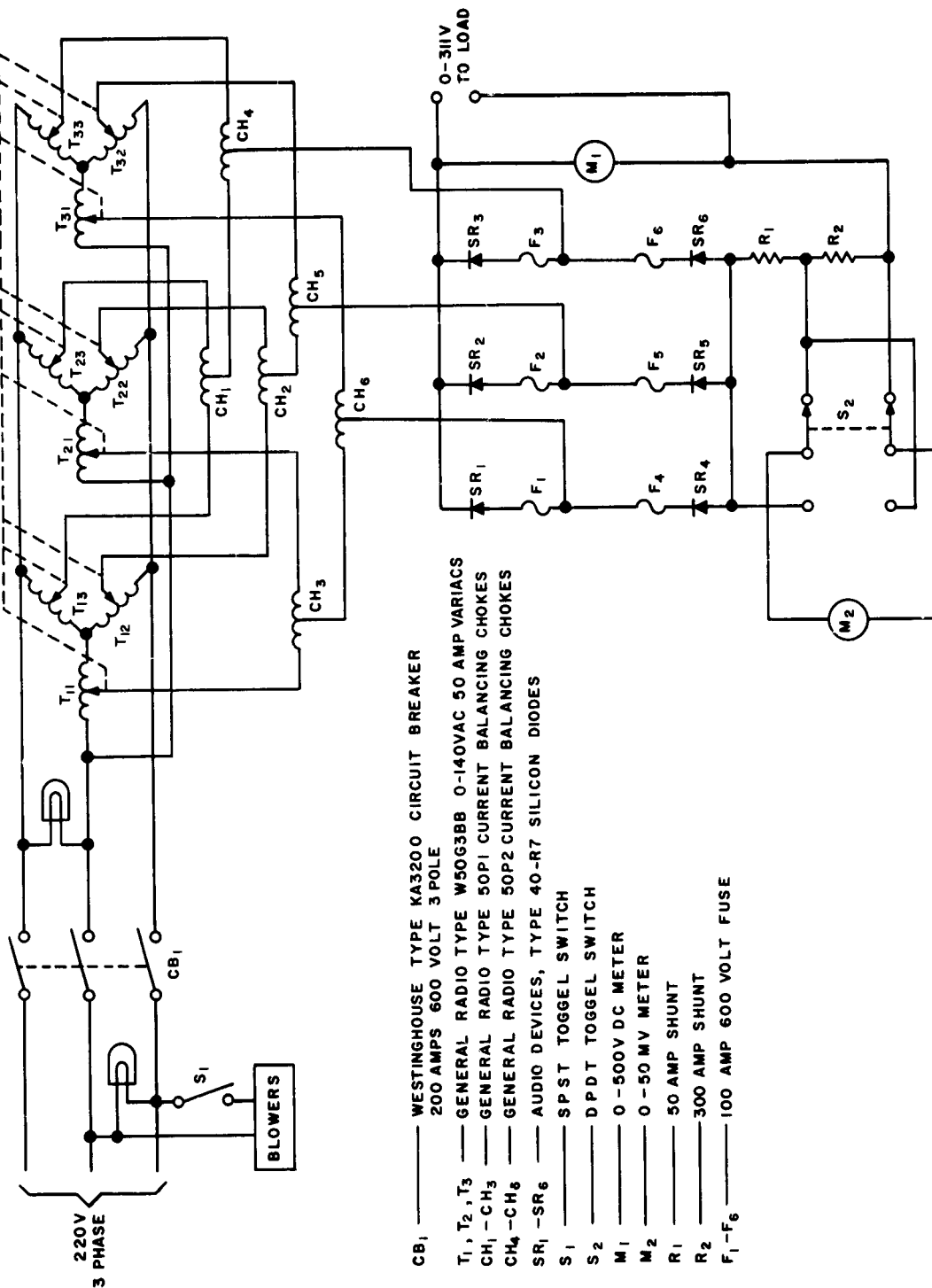


Figure 39. Magnet Supply Circuit

APPENDIX III

CESIUM FILAMENT SUPPLY CIRCUIT

The cesium filament supply circuit is shown in Figure 40. It provides two completely independent output voltages and a positive unblanking pulse having the phase relationship with the output voltage waveform shown in Figure 41. The voltmeter reads directly in rms volts while the current meters read dc amps. The latter reading must be multiplied by a factor of $2/\pi$ in order to obtain the rms current. The specifications for the power supply are given in Table IX. The supply is shown in Figure 42.

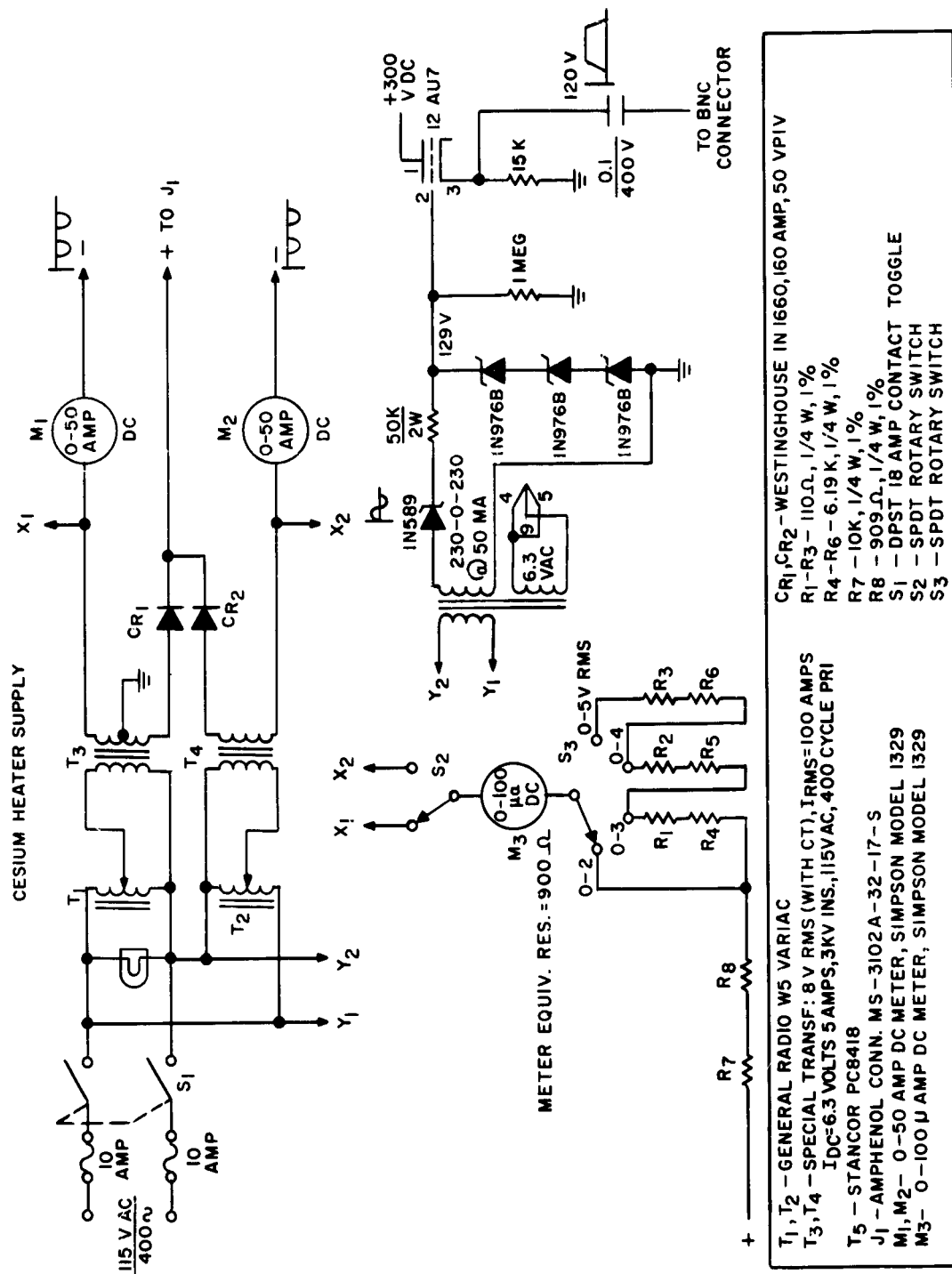


Figure 40. Cesium Filament Supply Circuit Diagram

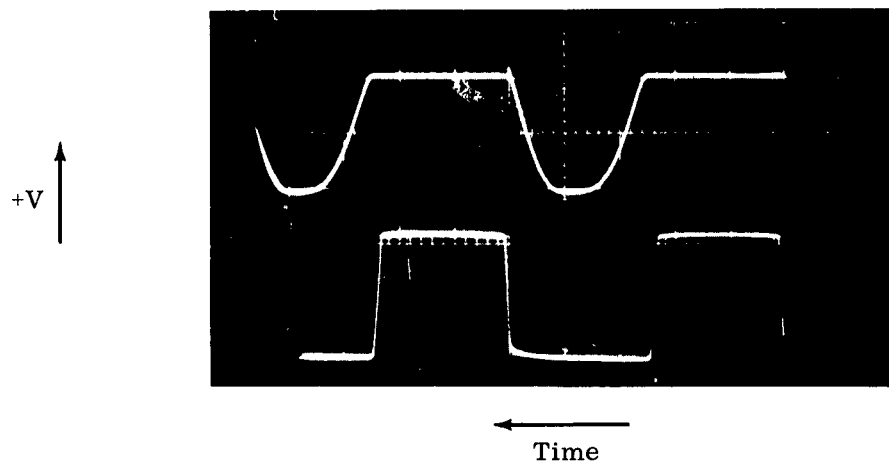


Figure 41. Cesium Filament Supply Output Waveforms

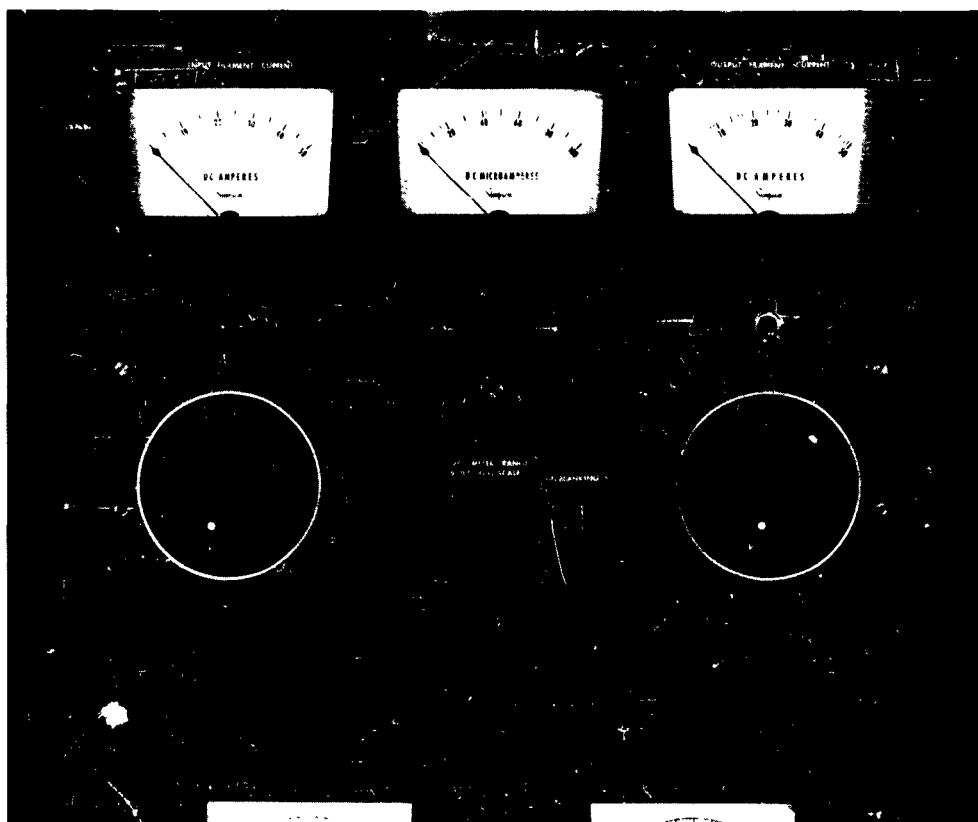


Figure 42. Cesium Filament Supply

TABLE IX

CESIUM FILAMENT SUPPLY SPECIFICATIONS

$V_{in} = 115 \text{ vac, 400 cycle}$

$V_{2 \text{ out}} = 0 - 5 \text{ vrms pulsating dc}$

$V_{1 \text{ out}} = 0 - 5 \text{ vrms pulsating dc}$

$I_{2 \text{ out}} = 0 - 100 \text{ amps rms}$

$I_{1 \text{ out}} = 0 - 100 \text{ amps rms}$

$V_{out} = 120 \text{ volts, 400-cycle square wave}$

APPENDIX IV

CATHODE ACTIVATION PROCEDURE

To activate the oxide cathode, the filament voltage is slowly raised to about 6.3 volts, at which point heavy outgassing is noted. From this point, the filament voltage is raised slowly to 9 volts, waiting at each voltage setting until the increased outgassing is overcome by the pump. When the pressure in the system finally returns to its initial value, the filament is "hot-shotted" to a filament voltage of about 12.5 volts for 30 seconds and then dropped to 8.8 volts. The latter voltage corresponds to a current of 1.4 amps. The cathode is allowed to age at 1.4 amps for 15 minutes. A positive voltage is then applied to the grid and increased until 10 ma is drawn. The current drawn is then increased by steps of 10 ma, with a period of 2 minutes at each current level. The cathode is aged for about 30 minutes with a current of 60 ma flowing to the grid.

The voltage is removed from the grid and a positive voltage is applied to the anode. This voltage is increased until an anode current of 8 ma is reached. The 8-ma current is drawn for a period of 30 minutes, thus outgassing the anode. To outgas the drift tube and input helix, the anode voltage is removed and a negative grid voltage is applied, helix voltage of 600 volts is applied, then the anode voltage reapplied and the grid voltage reduced until 5 ma is drawn to the drift tube, all of this with no magnetic field applied. Under these conditions, the voltage and currents are those given in Table X. Note that with no magnetic field applied, none of the beam gets beyond the input helix.

TABLE X

GUN VOLTAGES AND CURRENTS -- NO MAGNETIC FIELD

V_f	= 8.8 vac	I_d	= 5 ma
I_f	= 1.4 Amps ac	I_{ms}	= 350 μ a
V_a	= 607 volts	I_1	= 1.6 ma
I_a	= .1 ma	I_2	= 0 ma
V_g	= 13 vdc	I_c	= 0 ma
V_h	= 600 volts	I_t	= 8 ma

Note: This is the voltage at the power supply. The voltage at the filament is somewhat lower due to lead resistance.

APPENDIX V

STATISTICAL ANALYSIS OF HOT TUBE DATA

The hot tube data consisted of two measurements at each frequency. On the other hand, for the cold tube data two measurements were available only at the 100-mc points and at those points where overlap by the sets of measurements occurred. In the cases where two points existed, the standard deviation (σ) was calculated by the usual method. To estimate the standard deviation for those points where there was only a single measurement available, the standard deviation was taken as the mean of the standard deviation for the other points. In plotting the curves of Figures 33, 34 and 35, if the standard deviation for a point was less than the mean standard deviation, the mean standard deviation was plotted.

The t-test¹² was applied to the results in the following manner. If the quantities \bar{x}_1 and \bar{x}_2 , and σ_1^2 and σ_2^2 are means and variances, with variances of the mean $s_{\bar{x}_1}^2 = \sigma_1^2/n_1$ and $s_{\bar{x}_2}^2 = \sigma_2^2/n_2$. Then

$$t = \frac{\bar{d} - \delta}{\sqrt{s_{\bar{x}_1}^2 + s_{\bar{x}_2}^2}}$$

where $\bar{d} = \bar{x}_1 - \bar{x}_2$ and $\delta = \mu_1 - \mu_2$ has the "Student" t-distribution with v degrees of freedom. Here μ_1 and μ_2 are the "true" means of population 1 and population 2, respectively. The number of degrees of freedom is in turn given by

$$\frac{1}{\nu} = \frac{1}{\nu_1} \left(\frac{s_{\bar{x}_1}^2}{s_{\bar{x}_1}^2 + s_{\bar{x}_2}^2} \right)^2 + \frac{1}{\nu_2} \left(\frac{s_{\bar{x}_2}^2}{s_{\bar{x}_1}^2 + s_{\bar{x}_2}^2} \right)^2$$

where $\nu_1 = n_1 - 1$ and $\nu_2 = n_2 - 1$ are the number of degrees of freedom for σ_1^2 and σ_2^2 , respectively. This was the best test that we could find that was applicable to comparing two sets of measurements where both sets possess errors.

The chi-square test¹³ was applied to the over-all curve fit. It, however, is not truly applicable since it is designed to compare a measured curve with a theoretical curve or an expected curve. As a result, this test can give a result that says the data are significantly different when, in fact, they are not. We have not been able to find a test equivalent to the t-test, in the form given above, which will test for curve fit.

The large error in the data for the hot tube radiated signal relative to input signal and the transmitted signal relative to input signal is due to a large error in a conversion constant for converting the one-milliampere modulated (grid unblanking) data to an equivalent three-milliampere unmodulated (steady beam) value. This error can be eliminated in the future by making all measurements with the modulated beam, and by modifying the instrumentation slightly to ensure that the modulated beam current wave form is the same for all measurements.

From the statistical analysis of the data presented in the reports, certain worthwhile conclusions can be arrived at regarding the number of measurements required to reduce the uncertainty and increase the significance. Particularly important is the conclusion cited in the preceding paragraph and the fact that a minimum of 3 to 4 measurements are required for good results. The latter conclusion follows immediately from the observation that the significance for a given value of t rapidly increases with increasing ν . For example, at $t = 13$, for one degree of freedom the probability of the deviation being due to chance is $p = .05$; while for 2 degrees of freedom, $p = .01$ and for 3 degrees of freedom, $p = .001$.